Control Engineering Practice 130 (2023) 105375

Contents lists available at ScienceDirect

Control Engineering Practice

journal homepage: www.elsevier.com/locate/conengprac

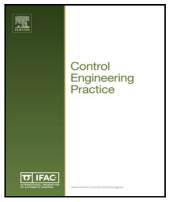

Automatic sea state estimation with online trust measure based on ship response measurements

Astrid H. Brodtkorb [a,*], Ulrik D. Nielsen [a,b]

[a] Centre for Autonomous Marine Operations (NTNU AMOS), Department of Marine Technology, Norwegian University of Science and Technology (NTNU), Otto Nielsens vei 10, 7052 Trondheim, Norway

[b] DTU Mechanical Engineering, Technical University of Denmark, DK-2800 Kgs. Lyngby, Denmark

ARTICLE INFO

Keywords:
Non-parametric sea state estimation
Wave-buoy analogy
Situational awareness
Autonomous ships
Linear discrete-time state estimation

ABSTRACT

The ever-changing sea state constitutes an integral part of situational awareness for vessels at sea. In this paper, a computationally efficient sea state estimation algorithm is extended by (1) automatic gain and tolerance calculation, and (2) trust measure for wave filtering condition identification. The resulting algorithm can run online in a control system without the need of user input, producing estimates of sea state parameters (significant wave height, peak wave frequency and main propagation direction), while simultaneously monitoring the quality of the estimates produced by identifying when wave filtering occurs. The algorithm is developed for application in dynamic positioning (DP) control systems, where the vessel has zero (or low) forward speed. The estimation method is tested with realistic values of measurement noise and sampling in terms of comprehensive time series simulations based on both long- and short-crested wave conditions. The sea state estimates correspond well with a state-of-the-art Bayesian estimation approach. This indicates that the simplifications made in order to enhance the computational speed, has not affected the quality of the estimates to any significant extent. The trust measure correctly identifies when wave filtering occurs in all simulated scenarios.

1. Introduction

In recent years, the level of autonomy for ships has increased, enabling radical changes in how ship operations are performed; from passenger ferries (Reddy et al., 2019), to networks of small self-operated vessels, designed to operate at sea for prolonged periods of time, automatically mapping and monitoring oceanographic phenomena (Billings et al., 2021; Dallolio et al., 2021b).

The ever-changing sea state constitutes an integral part of situational awareness for vessels at sea, both with respect to safety of personnel and equipment, and for an efficient operation. In addition the waves changes how the vessel responds, which again influences which control strategies that should be applied. For unmanned surface vessels (USVs) the prevailing and near-future sea state influences planning and execution of safe operations. This is especially important for autonomous vessels operating on their own at sea prolonged periods of time. Many control algorithms rely on information about the peak frequency of the waves, and indirectly also on the significant wave height. A sea state estimate can be direct input to an autonomous control system and to a decision support system for operators, either onboard or onshore. For a sea state estimate to be used directly in a risk-informed control system (Thieme et al., 2021) the estimate needs to be precise, consistent, and computationally efficient. Higher precision (usually) comes at a cost of using a higher fidelity estimation algorithm with higher computational footprint.

Estimating the sea state based on ship motion measurements, often referred to as the *wave-buoy analogy* has had considerable attention during the last two decades, and hence there is a multitude of approaches today, see Nielsen (2017) for a comprehensive summary. The majority of the past work has been formulated in the frequency-domain; either as Bayesian non-parametric approaches, enabling the estimation of the directional wave spectrum (Iseki & Ohtsu, 2000; Nielsen, 2005), or as parametric approaches, introducing an idealized directional wave spectrum (Montazeri et al., 2016; Simos et al., 2007; Tannuri et al., 2003). These approaches have a higher computational load due to the formulation of the wave spectrum estimation problem, and run *offline* in the sense that they analyze data in a post-process. Simpler formulations of the wave spectrum estimation problem based on optimization (Pascoal et al., 2007; Ren et al., 2021) or iterative procedures (Brodtkorb et al., 2018a; Nielsen et al., 2018) are much lighter computationally. The main difference between the algorithms is that the simplified formulation provides an estimate momentarily after a sufficient response data sequence has been gathered, since the computation time and effort is low.

* Corresponding author.
E-mail addresses: astrid.h.brodtkorb@ntnu.no (A.H. Brodtkorb), udni@mek.dtu.dk (U.D. Nielsen).

https://doi.org/10.1016/j.conengprac.2022.105375
Received 16 May 2022; Received in revised form 17 October 2022; Accepted 18 October 2022
Available online xxxx

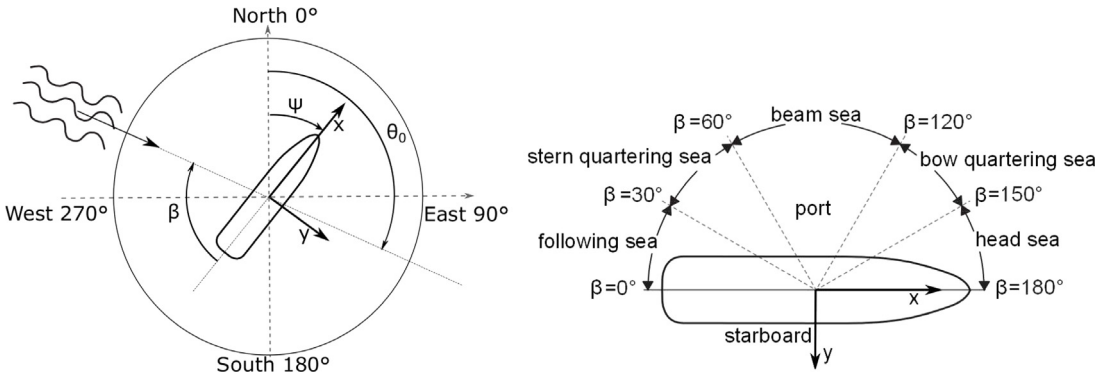

Fig. 1. Definition of the mean wave propagation direction $\Theta_0 \in [0, 360)^\circ$, heading of the vessel ψ, and relative wave direction β. Starboard incident waves have $\beta \in (-180, 0]^\circ$, and port incident waves have $\beta \in [0, 180]^\circ$.

The simultaneous use of multiple ships for sea state estimation has been investigated in Nielsen et al. (2019). There, the sea state estimates from the ships are obtained by the SSE algorithm formulated by Brodtkorb et al. (2018a). However, subsequently, the estimates from the individual ships are weighted as a function of their transfer functions, and the weighted wave spectrum estimate is more precise than the estimates from the individual ships alone.

It has been demonstrated that the *wave-buoy analogy* can be coupled with shipboard wave measurement systems, for instance wave radars (Stredulinsky & Thornhill, 2011), or wave probes installed on the hull of the vessel (Souza, 2019) for increased accuracy of the estimates, compared to the individual methods alone. In cases where the ship is large compared to the waves, the ship will act as a low-pass filter, taking away high-frequency wave components from the response. This phenomenon is a well-known, and well-studied, challenge when estimating waves using ship-borne sensors, see for instance Nielsen (2007), Souza (2019).

Simple time-domain approaches that estimate parts of the wave parameters include estimation of peak frequency on encounter (Belleter et al., 2015); which is verified on experimental data from an autonomous surface vehicle (Dallolio et al., 2021a), peak frequency and regular wave amplitude estimation (Nielsen et al., 2015), and wave direction estimation using Inertial Measurement Units (IMUs) distributed along a ship hull (Udjus, 2017). On the other end, methods based on Kalman filtering (Iseki, 2010; Pascoal et al., 2017) estimate all wave parameters, and are available at high update rates. There is also the possibility to reconstruct the incident wave profile based on short-time response measurements (Takami et al., 2022).

One weakness of the aforementioned approaches, including the one used in this paper, is that they all depend on accurate wave-to-motion transfer functions. Transfer functions themselves depend on the detailed hull geometry and loading condition, both of which are not always available. Tuning transfer functions by using ship motion data without relying on detailed hull geometry has been investigated in Han et al. (2021), Nielsen et al. (2021, 2022), and estimating the sea state and tuning transfer functions by using multiple ships simultaneously is proposed in Mounet et al. (2022). Approaches that are not dependent on accurate hull geometry and transfer functions are, for instance, multilayer random forest classifier (Cheng et al., 2019) and deep learning (Scholcz & Mak, 2020) and convolutional neural networks (Toshiki et al., 2021). Larger quantities of appropriately labeled training data for sea state estimation is difficult to come by, as training on measurements of ships in operation is preferred, and the sea state is in general not measured. Machine learning approaches have also been used for real-time wave estimation and prediction (Chen et al., 2021; Duz et al., 2021; Wu & Gao, 2021).

As the above literature overview indicates, there exists numerous methods for sea state estimation, and the choice of method is often affected by the engineering application needs. Some operations may require a time-domain estimate or prediction of the onsite sea state, whereas others are more concerned with the main wave parameters on a 30-minute basis.

1.1. Main contributions

This paper is an extension of the work in Brodtkorb et al. (2018a, 2018b), where the sea state estimation algorithm based on iteration was first proposed. The main contributions of this paper include automatic gain calculation and tolerance adjustments, and the proposal of trust measure, indicating when the sea state estimates are of good quality and when they are not. Moreover, an approach for correcting the wave direction estimate during heading changes is introduced. The resulting algorithm is computationally efficient, robust, does not require tuning for varying sea states, and is self-monitoring in terms of estimation quality. The algorithm is useful in online autonomous decision support and switching control systems.

The developed algorithm is tested in a comprehensive simulation study based on simulated response time series sequences. Tests and evaluations are made with the algorithm running *online* in a DP control system of three different vessels, in both short- and long-crested wave conditions. In addition a non-parametric (Bayesian) approach, see Nielsen (2008), is run on the same data set as a post-process in order to facilitate a benchmarking study with state-of-the-art sea state estimation procedures.

1.2. Organization of the paper

In Section 2, the underlying definitions and assumptions are given. The wave estimation procedure including automatic gain calculation, transient correction, and online trust monitoring is presented in Section 3. The simulation setup and results are presented and discussed in Section 4, and Section 5 concludes the paper.

2. Definitions and assumptions

For control design purposes, the vessel motion is usually modeled as a mass–damper-restoring system subject to the loads from current, wind, and waves (Fossen, 2011). For ships in DP the thrusters will produce mean and slowly varying generalized forces in the horizontal plane to cancel those from the environment. Therefore the DP control system influences the surge, sway and yaw motion of ships directly, and the *heave (z), roll* (ϕ) and *pitch* (θ) motions are more suited for sea state estimation. The measurements of heave, roll and pitch are recorded in the *body*-frame, which is defined with positive x-axis pointing towards the bow, positive y-axis pointing towards starboard, and with positive z-axis pointing down, see Fig. 1. In DP the vessel has zero or low forward speed, so that the frequency of encounter is assumed to be the same as the incident wave frequency, $\omega_e = \omega_0 = \omega$. To keep the

formulation of the sea state estimation algorithm as simple as possible, it is assumed that the waves are long-crested, with mean propagation direction Θ_0, as defined in Fig. 1. The wave direction relative to the vessel heading is β, with $\beta = 180°$ being head incident sea, and $\beta = 0°$ being following incident sea. A consequence of this is that the governing equation of motion can be simplified from a problem of finding the frequency-directional spectral density to a considerably simpler problem where the spectral density is only a function of frequency. Although the algorithm itself assumes long-crested waves, the algorithm is not prohibited from being used with realistic short-crested waves, cf. Section 4 (Table 2). The relationship between the wave amplitude and the vessel response amplitude (here only heave, roll and pitch are considered) is assumed to be linear, and given by the complex-valued (motion) transfer functions $X_i(\omega, \beta)$, which can be calculated using hydrodynamic software codes,[1] or alternatively estimated using Closed-form Expressions (Jensen, 2001), as demonstrated in Brodtkorb et al. (2018a) and Mounet et al. (2022). The complex-valued cross-spectra $R_{ij}(\omega)$ can be calculated as:

$$R_{ij}(\omega) = X_i(\omega, \beta)\overline{X_j(\omega, \beta)}S(\omega), \tag{1}$$

where $R_{ij}(\omega)$, $i, j = \{z, \phi, \theta\}$ are the heave, roll, and pitch response spectra, $\overline{X_j(\omega, \beta)}$ is the complex conjugate of the transfer functions in heave, roll and pitch for the relative wave direction β, and $S(\omega)$ is the wave spectrum. When $i \neq j$, $R_{ij}(\omega)$ is complex-valued, and when $i = j$ the imaginary part is zero, $\mathcal{I}m(R_{ii}(\omega)) = 0$. The imaginary parts of the cross spectra pairs have opposite signs, i.e., $\mathcal{I}m(R_{ij}(\omega)) < 0 \Leftrightarrow \mathcal{I}m(R_{ji}(\omega)) > 0$, that are dependent on the incident wave direction. This is used later to distinguish whether the waves are starboard or port incident, relying on the method formulated in Brodtkorb et al. (2018a).

For numerical stability of the estimation procedure, the magnitudes of Eq. (1) are considered, that is

$$\left|R_{ij}(\omega)\right| = \left|X_i(\omega, \beta)\overline{X_j(\omega, \beta)}\right| S(\omega), \;\; i, j = \{z, \phi, \theta\} \tag{2}$$

where

$$\left|R_{ij}(\omega)\right| = \sqrt{\left[\mathcal{R}e(R_{ij}(\omega))\right]^2 + \left[\mathcal{I}m(R_{ij}(\omega))\right]^2}. \tag{3}$$

In summary, the following fundamental assumptions are introduced:

(A1) The response spectra $R_{ij}(\omega)$ are computed based on *stationary* responses in heave, roll and pitch $i, j = \{z, \phi, \theta\}$.
(A2) The motion transfer functions $X_i(\omega, \beta), i = \{z, \phi, \theta\}$ are known.
(A3) The wave spectrum is stationary over the time span that is examined, i.e.,

$$S^+(\omega) = S(\omega), \tag{4}$$

where "+" denotes the *next discrete time step*.
(A4) The sea state can be described as long-crested.
(A5) The forward speed of the vessel is low, if not zero, so that $\omega_e = \omega_0 \equiv \omega$.

3. Automatic sea state estimation algorithm

The non-parametric sea state estimate, consisting of a wave spectrum estimate, a wave direction estimate, and a trust measure is computed in three steps, as illustrated by Fig. 2, and described in details in the following sections. The main estimation step, including the (initial) estimate of the wave direction, is the same as in the procedure outlined in Brodtkorb et al. (2018a, 2018b). It is repeated here for the sake of convenience, and in order to put the novel sections on gain calculations, trust measure formulation and transient correction into context.

The time series of heave, roll and pitch response are pre-processed by computation of response cross-spectra, and the gains and tolerances used in the estimation algorithm are calculated, see Section 3.3. The gains are dependent on the formulation of the main algorithm, so in the sections below, the main algorithm is presented first. The main estimation step is the computation of wave spectrum candidates $\hat{S}(\omega, k)$, established by solving Eq. (2) through iteration, see Section 3.1. In the post-processing step, the energy in the wave spectrum candidates are compared to get an energy-averaged direction estimate $\hat{\beta}$, and the wave spectrum estimate and its corresponding parameters, i.e., significant wave height $\hat{H}_s$, peak period $\hat{\omega}_p$, are computed, see Section 3.2. Methods for online trust monitoring and transient correction is presented in Section 3.4.

The estimation algorithm presented in this paper is of a modular nature, and therefore adding functionality for directional spread estimation, or forward speed can be done (Nielsen et al., 2018).

3.1. Main estimation step: Wave spectrum candidates

For each response pair $ij = \{zz, \phi\phi, \theta\theta, z\phi, z\theta, \phi\theta\}$ and for each discretized direction $k = \{0, \dots, 180\}$ and discretized frequency ω, repeat the following steps,

$$\hat{R}_{ij}(\omega, k) = \left|X_i(\omega, k)\overline{X_j(\omega, k)}\right| \hat{S}_{ij}(\omega, k) \tag{5a}$$

$$\tilde{R}_{ij}(\omega, k) = \left|R_{ij}(\omega)\right| - \hat{R}_{ij}(\omega, k) \tag{5b}$$

$$\hat{S}^+_{ij}(\omega, k) = \hat{S}_{ij}(\omega, k) + h_{ij}(\omega, k)\tilde{R}_{ij}(\omega, k) \tag{5c}$$

until a threshold is reached

$$\sum_{\omega} \left|\tilde{R}_{ij}(\omega, k)\right| \leq \epsilon_{ij}, \;\; \epsilon_{ij} > 0. \tag{6}$$

Eq. (5)a is a copy of the governing equation, see Eq. (2), Eq. (5)b is the driving error, and Eq. (5)c is a discrete-time linear Luenbeger-type observer. The iteration is computationally inexpensive and fast, and is performed for waves assumed to approach on one side of a port/starboard symmetric vessel. Since the relative wave direction is unknown initially, the wave spectrum candidate is dependent on the direction as well as frequency, $\hat{S}_{ij}(\omega, k)$. The gain $h_{ij}(\omega, k) > 0$ is a tuning parameter that is discussed in Section 3.3. The next value of the wave spectrum candidate is denoted $\hat{S}^+_{ij}(\omega, k)$.

The method does not assume a wave spectrum shape, or parametrize it in any way, and hence the initial wave spectrum estimate and estimate of the response spectrum are set to zero, $\hat{S}_{ij}(\omega, k) = 0$ and $\hat{R}_{ij}(\omega, k) = 0$.

With N_ω and N_β number of wave frequencies and directions, respectively, the output from Eq. (5) is organized in a wave spectrum candidate matrix of dimension $6 \times N_\omega \times N_\beta$,

$$\bar{S} = \begin{bmatrix} \hat{S}_{zz}(\omega, 0) & \dots & \hat{S}_{zz}(\omega, k) & \dots & \hat{S}_{zz}(\omega, 180) \\ \hat{S}_{\phi\phi}(\omega, 0) & \dots & \hat{S}_{\phi\phi}(\omega, k) & \dots & \hat{S}_{\phi\phi}(\omega, 180) \\ \hat{S}_{\theta\theta}(\omega, 0) & \dots & \hat{S}_{\theta\theta}(\omega, k) & \dots & \hat{S}_{\theta\theta}(\omega, 180) \\ \hat{S}_{z\phi}(\omega, 0) & \dots & \hat{S}_{z\phi}(\omega, k) & \dots & \hat{S}_{z\phi}(\omega, 180) \\ \hat{S}_{z\theta}(\omega, 0) & \dots & \hat{S}_{z\theta}(\omega, k) & \dots & \hat{S}_{z\theta}(\omega, 180) \\ \hat{S}_{\phi\theta}(\omega, 0) & \dots & \hat{S}_{\phi\theta}(\omega, k) & \dots & \hat{S}_{\phi\theta}(\omega, 180) \end{bmatrix}. \tag{7}$$

3.2. Post-processing step: Energy-averaged wave direction

The relative wave direction is an *energy-averaged* direction estimate found by comparing the significant wave height H_s estimate for each of the wave spectra candidates in $\bar{S}$. The result is collected in a matrix with dimensions $6 \times N_\beta$,

$$\bar{H}_s = \begin{bmatrix} H_{zz}(0) & \dots & H_{zz}(k) & \dots & H_{zz}(180) \\ H_{\phi\phi}(0) & \dots & H_{\phi\phi}(k) & \dots & H_{\phi\phi}(180) \\ H_{\theta\theta}(0) & \dots & H_{\theta\theta}(k) & \dots & H_{\theta\theta}(180) \\ H_{z\phi}(0) & \dots & H_{z\phi}(k) & \dots & H_{z\phi}(180) \\ H_{z\theta}(0) & \dots & H_{z\theta}(k) & \dots & H_{z\theta}(180) \\ H_{\phi\theta}(0) & \dots & H_{\phi\theta}(k) & \dots & H_{\phi\theta}(180) \end{bmatrix}. \tag{8}$$

with

$$H_{ij}(k) = 4\sqrt{m_{0,ij}}, \quad m_{0,ij} = \int_0^\infty \hat{S}_{ij}(\omega, k)d\omega \tag{9}$$

[1] Here ShipX (Sintef Ocean, 2017) is used.

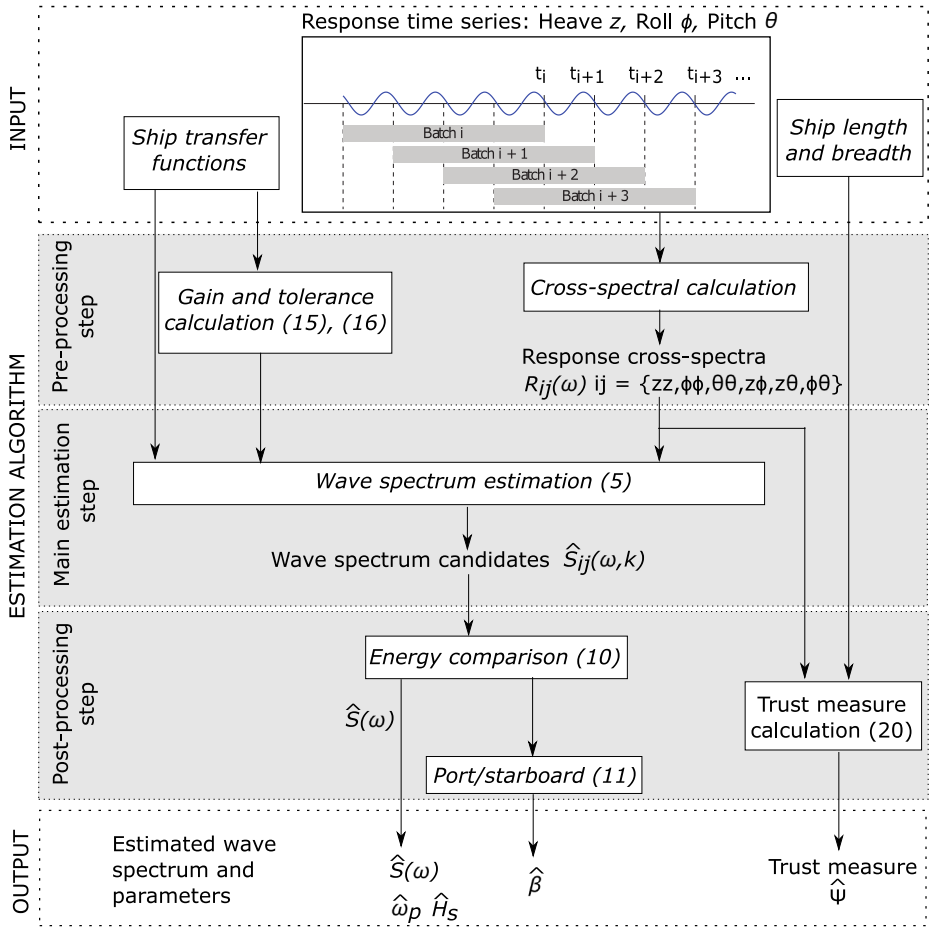

Fig. 2. Illustration of the proposed sea state estimation method, in three steps. Firstly cross-spectra and algorithm gains and tolerances are calculated. Then the wave spectrum candidates are calculated in the main estimation step, and finally the energy-averaged direction, spectral parameters, and trust measure are calculated. Numbers in parenthesis refer to equation numbers.

for each $ij = \{zz, \phi\phi, \theta\theta, z\phi, z\theta, \phi\theta\}$. For each direction k, the variance of $H_{ij}(k)$ is calculated, and the direction estimate is taken as the column of $H_{ij}(k)$ with the lowest variance

$$\alpha = \arg\min_k \left(\text{var}(H_{ij}(k))\right). \tag{10}$$

Since the iteration Eq. (5) is done for waves incident on one side of the hull, $\alpha \in [0, 180]$. The direction estimate is corrected for port/starboard incident sea state by using the imaginary part of the heave-roll cross spectra $\mathcal{I}m(R_{z\phi})$, which has opposite sign for port (PT) and starboard (SB) incident sea.

$$\hat{\beta} = \begin{cases} \alpha, & \text{when } \int_{\omega=0}^{\omega_N} \mathcal{I}m(R_{z\phi}(\omega))d\omega < 0 \quad (\text{PT} \in [0, 180]) \\ -\alpha, & \text{when } \int_{\omega=0}^{\omega_N} \mathcal{I}m(R_{z\phi}(\omega))d\omega \geq 0 \quad (\text{SB} \in (-180, 0)). \end{cases} \tag{11}$$

where ω_N is the highest frequency.

From previous studies (Brodtkorb et al., 2018b), it is found that examining the energy in the wave spectrum candidates is sometimes not sufficient to distinguish head from following sea in smaller sea states, especially if shorter time series of the vessel response is considered. Therefore a correction for head/following sea is made in a similar way to port/starboard by using the imaginary part of the heave pitch cross-spectra $\mathcal{I}m(R_{z\theta}(\omega))$.

$$\hat{\beta} \in \begin{cases} (0, 90), & \text{when } \int_{\omega=0}^{\omega_N} \mathcal{I}m(R_{z\theta}(\omega))d\omega < 0 \\ [90, 180], & \text{when } \int_{\omega=0}^{\omega_N} \mathcal{I}m(R_{z\theta}(\omega))d\omega \geq 0. \end{cases} \tag{12}$$

The wave spectrum estimate is taken as the spectral estimate in heave for the direction estimate,

$$\hat{S}(\omega) = \hat{S}_{zz}(\omega, |\hat{\beta}|). \tag{13}$$

The reason is that the estimate using the heave response has been found to be the most consistent (Brodtkorb et al., 2018a), and, for *online* implementation, update rate is important as well as robustness, accuracy and consistency. In principle this could be taken as the mean of the sea state estimates for all responses. $\hat{H}_s$ and $\hat{\omega}_p$ are calculated as

$$\hat{H}_s := 4\sqrt{m_0}, \quad m_0 := \int_0^\infty \hat{S}(\omega)d\omega \tag{14a}$$

$$\hat{T}_p := \frac{2\pi}{\hat{\omega}_p}, \qquad \hat{\omega}_p := \arg\max_\chi \hat{S}(\omega_\chi). \tag{14b}$$

3.3. Pre-processing step: Autotuning of gains h_{ij} and tolerances ε_{ij}

A stability analysis of the main estimation step was presented in Brodtkorb et al. (2018b), see a summary in Appendix. This resulted in the following restrictions on the gains

$$h_{ij}(\omega, k) < \frac{2}{\left|X_i(\omega, k)\overline{X_j(\omega, k)}\right|}, \; ij = \{zz, \phi\phi, \theta\theta, z\phi, z\theta, \phi\theta\},$$

in order to have a stable sea state estimator. The values of the gains are functions of the vessel transfer functions, which are case specific; depending on the vessel considered and its operating conditions (main dimensions, draught, forward speed, etc.). They are also dependent on the wave frequency and direction. By taking the maximum values of the motion transfer functions with respect to wave frequency and direction, the formulation becomes

$$h_{ij} < \frac{2}{\max_\omega \left(\max_k \left|X_i(\omega, k)\overline{X_j(\omega, k)}\right|\right)} < \frac{2}{\left|X_i(\omega, k)\overline{X_j(\omega, k)}\right|}.$$

Hence, the gains are chosen as

$$h_{ij} = \kappa h_{ij,max} = \kappa \frac{2}{\max_{\omega} \left(\max_{k} \left| X_i(\omega,k) \overline{X_j(\omega,k)} \right| \right)}, \tag{15}$$

with $\kappa \in (0,1)$. The gains auto-adjust with each vessel and conditions. A low gain will give a slower convergence rate of the state estimator, and a high gain will give faster convergence, but with the chance of inducing overshoot and/or oscillations. Notice that, in principle the gains are also dependent on the wave frequency and relative wave direction, however, preliminary simulation studies leading up to this work showed that there was not much to earn computationally, nor with regards to the final estimation error $\tilde{R}$. Therefore, the gains were left to be scalar quantities.

The tolerances ε_{ij} are chosen relative to the maximum value of the response spectra,

$$\varepsilon_{ij} = \delta \max_{\omega} \left(R_{ij}(\omega) \right), \tag{16}$$

where $\delta > 0$ is a small value. If ε_{ij} is too high, the iteration is terminated before information is passed from the response spectrum estimation error to the wave spectrum estimate. If the tolerance is too small, the iteration may not terminate. In directions where the transfer function magnitudes are small, the iteration procedure may get stuck before the threshold ε_{ij} is reached. This is typically the case for roll in head/following sea and pitch in beam sea. In these cases the ill-posed iteration is terminated.

3.4. Online trust monitoring and transient correction

The quality of a given sea state estimate $\{\hat{S}(\omega); \hat{H}_s, \hat{T}_p, \hat{\beta}\}$ is affected by a number of factors; some of which are easy to quantify and control, and others which may be more difficult to assess. It is important to have an estimate of the quality of the sea state estimate output, especially if it is to be used directly in supervisory switching controllers. In this section, two issues deteriorating the sea state estimate are dealt with: Firstly, a sea state trust measure is proposed for indication of whether the sea state estimates are degraded by *wave filtering*. Secondly, a strategy for minimizing the transients from heading changes on the relative wave direction estimate is proposed.

3.4.1. Trust measure $\hat{\Psi}$

Considering ship motions, e.g. heave, roll, pitch, the measured response spectrum $\hat{R}_{ij}$ will be missing information at the high-frequency tail, as the vessel acts as a low-pass filter (Nielsen, 2007). The main idea with the trust measure is to identify when the vessel is filtering out wave information, so that the user (or control system) will know when to trust the sea state estimate from the algorithm, and when to not. A preferred, yet sometimes impractical, solution to the wave filtering problem is to add a second sensor that is sensitive to smaller wave lengths, for instance wave probes, see Souza (2019).

Wave filtering occurs when the waves are short in comparison to the *vessel size corrected for the incident wave direction*. This quantity is introduced as the projected length W, expressed as

$$W = L|\cos(\beta)| + B|\sin(\beta)|, \tag{17}$$

where L is the ship length and B is the ship breadth, and β is the relative wave direction, see Fig. 3 for an illustration. The projected length is discussed to some detail in Dirdal et al. (2022).

In a spectral representation of a sea state, the wave component with the highest energy density has oscillation period T_p. Assuming infinite water depth, the wave length λ of this component is

$$\lambda = \frac{g}{2\pi} T_p^2, \tag{18}$$

where g is the acceleration of gravity. In principle, other characteristic periods of the sea state could also be used, for instance the middle

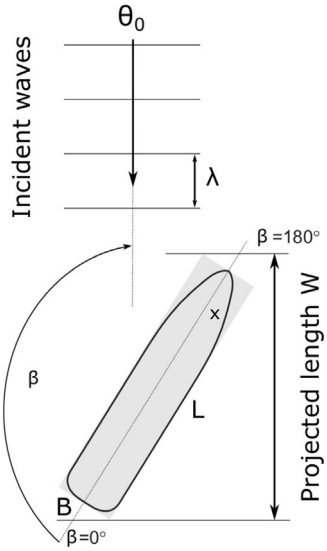

Fig. 3. Illustration of the projected length of the vessel W. The incident waves have characteristic wave length λ and mean wave propagation direction Θ_0.

period T_m or the mean zero-crossing period T_z. The period used would influence the values of the characteristic wave length somewhat. The wave filtering indicator, Ψ, is taken as the difference between the wave length and projected vessel length, normalized by the main dimensions of the vessel.

$$\Psi = \frac{\lambda - W}{\sqrt{L^2 + B^2}} \tag{19}$$

If Ψ is large, then wave filtering is likely not occurring. In this case the waves are long relative to the vessel projected length W. A low value of Ψ gives a relatively high chance of wave filtering, since there are some wave components that have shorter wave lengths λ than W. A negative value of Ψ indicates that wave filtering is occurring since then a significant number of wave components have wave lengths shorter than the vessel projected length.

Notice in Eq. (19) that Ψ is a function of wave parameters that need to be estimated; $\hat{T}_p$ and $\hat{\beta}$. If (19) is used directly as the trust measure, the trust measure will be dependent on the estimated parameters. This is not an ideal solution, as then bad estimates may deteriorate the trust measure as well. Therefore, the proposed trust measure is

$$\hat{\Psi} = \frac{\hat{\lambda} - L}{L} = \left(\frac{g T_{p3}^2}{2\pi L} \right) - 1, \tag{20}$$

where T_p in the expression for the characteristic wave length, Eq. (18), is substituted with the peak period of the heave response, T_{p3}. The heave response spectrum will in most cases, for zero forward speed, have a peak period in the vicinity of the peak wave period. In the case of non-zero forward speed, the heave response will not give a direct estimate of the peak wave period. Then another substitute for T_p could be made by estimating the encounter period by for instance using the roll motion (Belleter et al., 2015). The projected length W is simply substituted for the maximum value, $W = L$, which occurs in head/following sea (assuming $L > B$). The normalization is changed to just include the vessel length. In the case where a reliable relative wave direction is available, for instance based on cameras or other sensors that are not degraded by wave filtering, the projected ship length could be used directly. This would give a trust measure with realistic sensitivity to the relative wave direction.

3.4.2. Transient direction correction

The sea state parameters change slowly, however, the response data for the vessel may change rapidly due to a commanded heading (or

speed) change. This introduces unwanted transients in the response data sets, resulting in a violation of the assumption (A1) of stationary input data. It would be advantageous to detect when a transient occurs, and correct for this effect pro-actively when there is a commanded heading change. The desired yaw rate will be non-zero when there is a commanded heading change, e.g., $|r_d| > 0.001$ [rad/s], and for some time afterwards, since it takes some time for the transient to travel through the response cross-spectral estimation, as illustrated in Fig. 2. An estimate of the time it takes before a transient in the response signal is eliminated completely from the calculated response cross-spectrum is

$$T_{tr} = N_{FFT}\frac{1}{f_s}\left(\frac{100-\mu}{100}\right)N_{avg}, \tag{21}$$

where N_{FFT} is the number of samples used in the spectral calculation, f_s is the sampling frequency in Hertz, μ is the overlap of the data set in percent, and N_{avg} is the number of spectral estimates that are averaged for the final result. A flag is raised when the desired yaw rate $|r_d| > 0.001$ [rad/s], as then there will be data from a heading change transient in the cross-spectral calculation.

After a commanded heading change, some of the response data entering the cross-spectral calculations will be with the initial heading, and some of the response data will be with the final heading. This will make the estimated wave direction in the estimation algorithm lag. Therefore, the estimated wave direction is corrected using the measured heading of the vessel during the transient (T_{tr} seconds) according to

$$\hat{\beta}_{corr}(t) = \hat{\beta}(t) + b(\psi(t_0) - \psi(t)) \tag{22}$$

where t_0 is the time that the heading change starts, $\hat{\beta}(t)$ is the uncorrected relative wave direction estimate, $\psi(t_0)$ is the heading of the vessel at the time the heading change is commanded, and $\psi(t)$ is the measured heading at the current time instance. Due to the nature of the response cross-spectral calculations, the influence of the initial heading will be the largest for the first $\frac{1}{2}T_{tr}$ seconds, and will be smaller for the second half of the response, from $\frac{1}{2}T_{tr} - T_{tr}$ seconds. The constant b phases out the heading correction in a simple way with $b = 1$ when $t \in [t_0, t_0 + \frac{1}{2}T_{tr}]$ and $b = \frac{1}{2}$ when $t \in [t_0 + \frac{1}{2}T_{tr}, t_0 + T_{tr}]$. Section 4.1.2 contains an in-depth discussion of the cross-spectral parameters.

4. Results and discussion

In this section an extensive simulation study of the automatic sea state estimation algorithm is presented, and the results are discussed. Furthermore, the results are benchmarked against the Bayesian-based sea state estimation method described in Nielsen (2008).

4.1. Simulation setup

The sea state estimation algorithm is implemented in a comprehensive time-domain simulation model of a vessel in DP; including first-order wave-induced motions and mean and slowly varying wave drift motions, nonlinear Coreolis terms, nonlinear damping, fluid memory and fully coupled motions in six degrees of freedom. The DP control system features a nonlinear passive observer with time-varying gains (Værnø et al., 2017) for state estimation of surge, sway and yaw motions used in feedback with a nonlinear PID controller with reference feedforward. Measurement signals are sampled and noise is added for realistic measurements. Simulated time series of heave, roll and pitch motion are used as input to the sea state estimation procedure. The motion of three different ships, see Table 1 for main dimensions, are simulated for a DP maneuver where the ship makes successive heading changes of 30 degrees followed by longer periods of steady state; starting in head waves ($\beta = 180°$), followed by bow-quartering wave ($\beta = 150°$), etc. The response data generation and sea state estimation algorithm uses the same motion transfer functions calculated for the vessels using the linear strip theory code ShipX (Sintef Ocean, 2017). Hence, the estimation results obtained can be considered as the best possible, with no uncertainty introduced in the motion transfer functions. Here there are $N_\beta = 19$ directions, $k = \{0, 10, \dots, 170, 180\}$, and $N_\omega = 61$, $\omega = \{0.1, 0.15, \dots, 3.05, 3.1\}$ frequencies. It is noteworthy that the ships are considered individually/separately for making estimates of the sea state.

Table 1
Main ship parameters for Research Vessel (RV), Platform Supply Vessel (PSV), and Supply Vessel (S175).

Parameter	RV	PSV	S175
Length, L_{pp}	28.9 m	80 m	175 m
Breadth, B	9.6 m	17.4 m	25.4 m
Draught, T	2.63 m	5.6 m	9.5 m

Table 2
Summary of generating wave spectrum parameters for the different simulation cases.

Generating spectrum type	JONSWAP
Significant wave height	$H_s = 4$ m
Peak period	$T_p = \{8, 10, 12, 14, 16, 18\}$ s
Peakedness	$\gamma = 3.3$
Mean wave direction	$\Theta_0 = 180°$ (towards South)
Directional spread	$s = \{2, 50\}$
Number of wave components	200
Number of random directions	10
Number of wave realizations	10

4.1.1. Sea state parameters

The incident sea state is characterized by a JONSWAP spectrum, where the significant wave height $H_s = 4$ m, peakedness $\gamma = 3.3$, and mean wave direction $\Theta_0 = 180°$ (waves traveling South). Table 2 contains a summary of the incident wave parameters. The directional spread is computed as

$$D(\Theta) = \begin{cases} K_{2s}\cos^{2s}(\Theta - \Theta_0), & \text{for } -\frac{\pi}{2} < \Theta < \frac{\pi}{2} \\ 0, & \text{otherwise,} \end{cases} \tag{23}$$

with $s = \mathbb{Z}^+$, $K_{2s} = \frac{2^{2s-1}s!(s-1)!}{\pi(2s-1)!}$ and Θ_0 being the mean direction of the waves. The peak period $T_p = \{8, 10, 12, 16, 18\}$ s and directional spread $s = \{2, 50\}$ are changed from case to case. When $s = 50$ the sea state is close to long-crested, and when $s = 2$ the sea state is short-crested. Furthermore, to generate a realistic wave elevation time series, 200 wave components were used with 10 number of directions, picked from the directional spread distribution. Ten different wave elevation realizations were simulated per case to get some statistical data to work with. This gives 840 (7 relative wave directions, 6 peak periods, 2 directional spreads, 10 wave realizations) simulation scenarios to work with, when including the different relative wave directions induced by the heading changes.

Although the simulated response is not totally linear, due to nonlinear Coriolis, nonlinear damping, and fluid memory, it was found through initial studies that the significant wave height estimate was not influenced much by increasing the significant wave height of the waves. Therefore the incident H_s was left constant in this study. The simulator generating the vessel response is only valid for smaller sea states, where linear wave loads dominate the wave-induced response, which means that no slamming, water entry/exit, etc, are taken into account, and as such studying the effects of severe sea states on the algorithm performance is out of scope of the present study.

4.1.2. Cross-spectral calculation parameters

The cross-spectra are calculated using a Matlab/Simulink block based on Welch cross-spectral estimation method (Welch, 1967) using the parameters in Table 3. The Welch method is a computationally fast way to calculate the cross-spectra, and is hence a common choice. The choice of parameters for the cross-spectral calculation has great

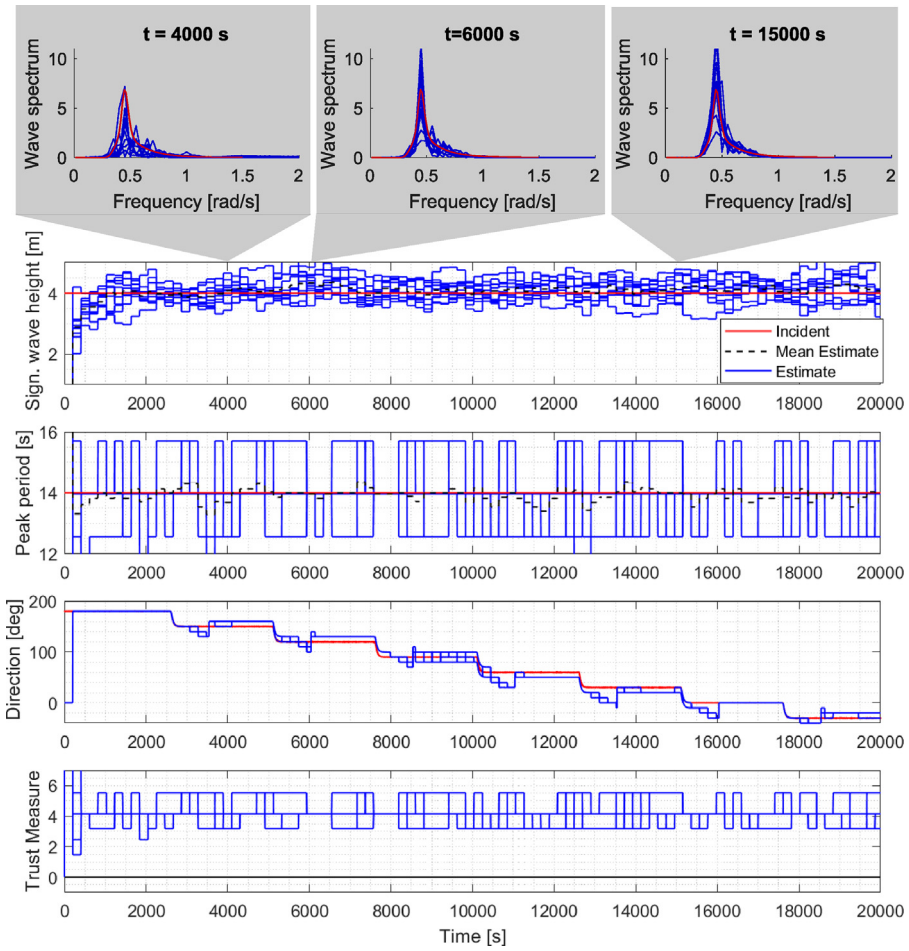

Fig. 4. Sea state estimation results for 10 realizations, PSV $T_p = 14$ s, spread $s = 50$, long-crested sea. At the top are wave spectra for three selected times. The next four subplots show the time series of the estimated significant wave height, peak period, relative wave direction and trust measure.

influence on the obtained sea state estimation results, so they should be chosen with care. The first issue is mitigating spectral leakage, since this is important for energy conservation and good estimates of the significant wave height. In Dah-Jing Jwo (2021), a Hamming window is suggested for having good spectral energy conservation properties, and so this is applied here. The next parameter to choose is the number of samples to be used in the FFT; N_{FFT}. Too short time window gives oscillatory (not consistent) estimates, whereas too long time window gives very long lag, which is not suitable for online applications. It was found, through trial and error, that $N_{FFT} = 1024$ was the lower limit for acceptable response cross-spectra with the ships and selected wave periods. For the results in the paper $N_{FFT} = 4096$ was used, however fewer samples, for instance $N_{FFT} = 2024$ also gives reasonable results; it is up to the user how frequent the updates should be versus how oscillatory estimates are tolerable. In general, there should be a minimum number of wave periods within the sample data to get a good representation of the signal using Fourier components. Since the peak period of the waves changes, N_{FFT} could in principle change for the different cases. However, changing this online is not recommended; N_{FFT} changes the shape (peakedness) of the response cross-spectra, and has a lot to say for the significant wave height estimate. Using a data overlap of 50% was found to give sufficiently smooth response spectra to work with, while at the same time emphasizing the most recent data points, relative to the history. It was found that taking the average of four consecutive spectra yielded good results.

Filling the cross-spectral calculation values from Table 3 into Eq. (21) to calculate the time it takes before a transient is completely eliminated from the response cross-spectral calculations, gives $T_{tr} = 820$ s (13 min). Because the response spectra are calculated with $N_{FFT} = 4096$ samples, and collected with $\mu = 50\%$ overlap, then the sea state estimation algorithm gives updates every $N_{FFT}\mu\frac{1}{f_s} = 202,4$ s (3,3 min).

Table 3
Summary of the parameters for cross-spectral calculation and estimation algorithm.

Cross spectra	Number of samples in FFT	$N_{FFT} = 4096$
	Sampling frequency	$f_s = 10$ Hz
	Number of spectral averages	$N_{avg} = 4$
	Percentage of data overlap	$\mu = 50\%$
Estimation algorithm	Gains	$h_{ij} = 0.9\frac{2}{\max_{\omega}\left(\max_{k}\lvert X_i(\omega,k)\overline{X_j(\omega,k)}\rvert\right)}$
	Tolerances	$\varepsilon_{ij} = 0.01\max_{\omega} R_{ij}(\omega)$
		$ij = \{zz, \phi\phi, \theta\theta, z\phi, z\theta, \phi\theta\}$

4.1.3. Auto-tuning of gains and tolerances

The method for auto-tuning gains and tolerances based on the vessel transfer functions works well, in the simulation scenarios tested. The algorithm was not tuned in between the cases, making it low-effort to adapt to different vessels. Different choices of $\kappa \in [0.5, 0.9]$ and $\delta \in [0.01, 0.1]$ were investigated. The algorithm performance was good for the investigated parameters, and more importantly the algorithm obtained estimation results for all combinations of κ, δ above. The computation time[2] of the algorithm (including the calculation of response

[2] Simulations were run in Matlab/Simulink on a Intel(R) Core(TM) i7-7700 CPU @ 3.60 GHz. The code was not optimized for speed in this implementation.

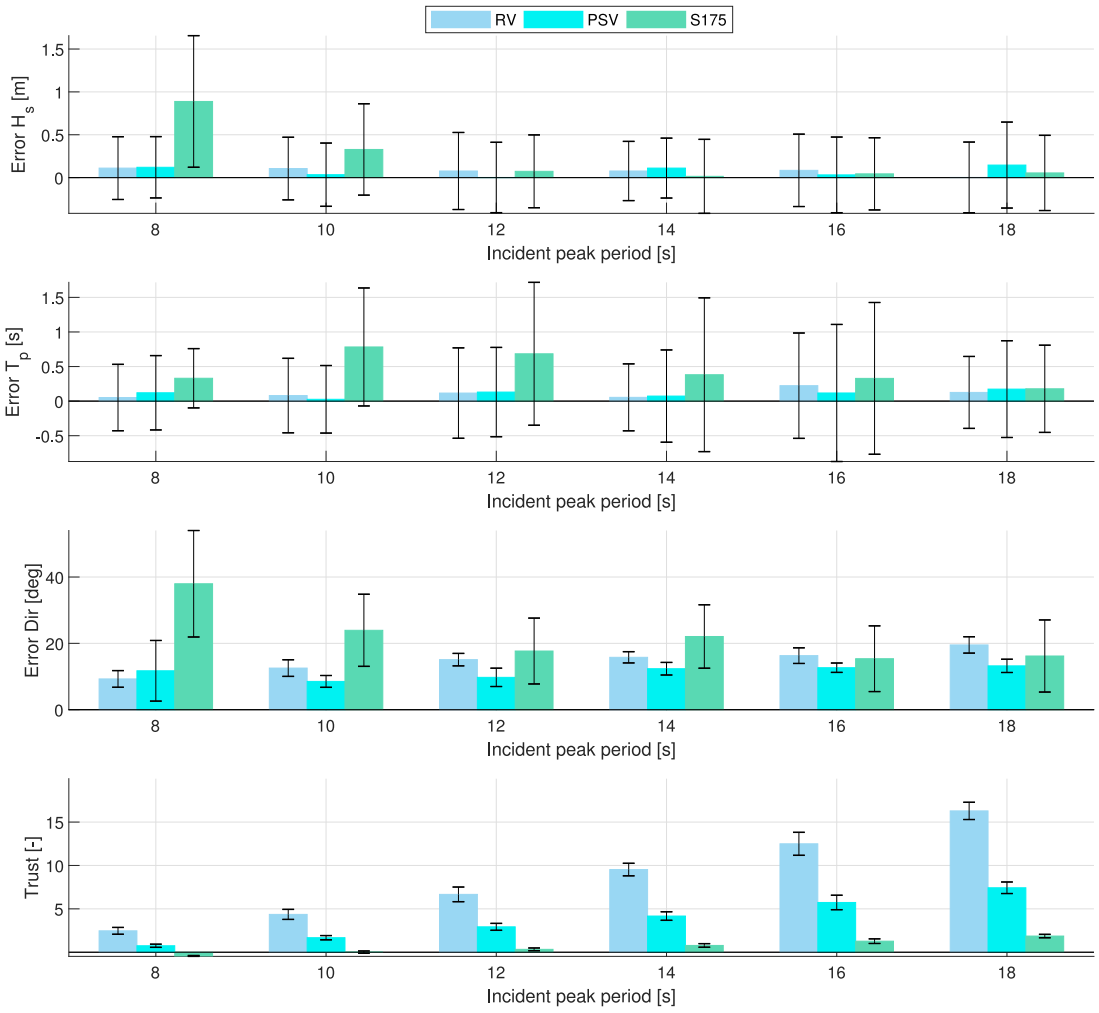

Fig. 5. Mean absolute estimation error and standard deviation for 10 realizations. Directional spread = 50 (long-crested sea). Mean and standard deviation are computed from time series 2000–20000 s.

spectra and gains, main estimation loop and post-processing) was less than 0.3 s for computing $(\hat{S}; \hat{H}_s, \hat{T}_p, \hat{\beta}, \hat{\Psi})$. The most time consuming part of the estimation procedure is by far computing the cross-spectra, and saving the estimation results to the matlab workspace. More interestingly, the algorithm is easy to implement, with few lines of code (80 lines in our non-optimized version, including comments), the gains and tolerances are auto-tuning, and the algorithm is robust, as shown through the numerous simulation cases presented in the following. The fact that the algorithm is capable of running without user input and being extremely efficient, makes it applicable in low-cost computers on board autonomous surface vessels.

4.2. Estimation results on simulated response

Fig. 4 shows the estimated sea state parameters $(\hat{S}; \hat{H}_s, \hat{T}_p, \hat{\beta}, \hat{\Psi})$ for PSV in $T_p = 14$ s, long-crested waves, plotted against time for all ten wave realizations (blue curves). The wave spectra $\hat{S}$ for three different times are also shown at the top. The mean $\hat{H}_s$ and, $\hat{T}_p$ for these scenarios are plotted with the black dashed line.

Descriptive statistics of the outcomes, all three ships considered, are summarized for the long-crested cases in Table 4 and for the short-crested cases in Table 5. A bar chart representation of the mean absolute estimation errors and trust measure for the long-crested cases is shown in Fig. 5, and for the short-crested cases in Fig. 6.

The mean and standard deviation are calculated for the time 2000–20000 s of the response, which gives time for the initial transients (0–2000 s) to die out. It is emphasized that the transient response due to heading changes is included in the mean and standard deviation values.

Recall that the trust measure $\hat{\Psi}$, defined in Eq. (20), is negative when wave filtering is occurring, and positive by some margin when there is no (or little) influence of wave filtering. The general trend is that when $\hat{\Psi} > 2$, the influence of wave filtering on the results are low; as there seems to be better quality in the estimation results when $\hat{\Psi} > 2$. The peak period estimate $\hat{T}_p$ is consistent (low standard deviation) and precise (low error) throughout, even for the cases when wave filtering is occurring. The same cannot be said for the significant wave height and direction estimates, see discussion in Section 4.2.1. The reason for the good results in $\hat{T}_p$ is likely that the peak period does not depend on the shape of the spectrum. If another period had been considered, e.g., the mean zero-crossing period $T_z = 2\pi\sqrt{(\frac{m_0}{m_2})}$, the results may be different. This is because T_z is calculated from the second spectral moment $m_2 = \int w^2 S(w) dw$, where the frequency is squared, making good estimation of the high-frequency tail of the spectrum important. In general it is the high-frequency tail of the wave spectrum that is the most difficult to approximate correctly using ship motions due to wave filtering.

When $\hat{\Psi} > 2$, the significant wave height estimate $\hat{H}_s$ is generally within 0.1 m (2.5%), $\hat{T}_p$ is within 0.2 s of the incident period, and the direction estimate $\hat{\beta}$ is generally within 13° in the long-crested case, and 16° in the short-crested case. Notice that the direction has a resolution of 10°, so this estimation error will naturally be larger than for the other parameters.

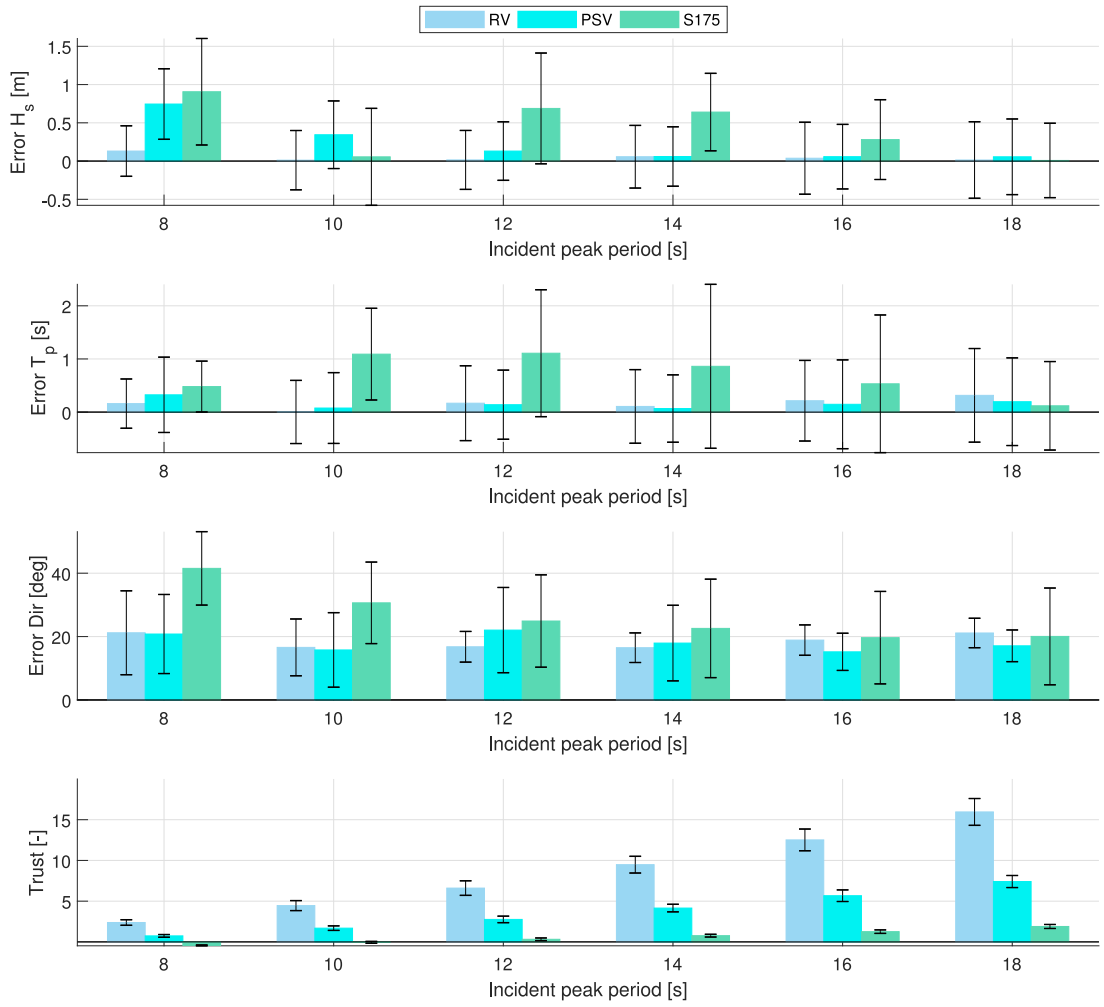

Fig. 6. Mean absolute estimation error and standard deviation for 10 realizations. Directional spread = 2 (short-crested sea). Mean and standard deviation are computed from time series 2000–20000 s.

It should also be acknowledged that the datasets presented in this paper include a high percentage of data during heading changes. There is a new heading change commanded every 2500 s. Of these it takes the vessel around 120 s to get to the new heading setpoint, and it takes $T_{tr} = 820$ s before the data from the transient is completely eliminated from the cross-spectral calculations. This leaves about 1560 s of steady state response at every relative wave direction, which is 60% of the total time. If only the steady state part of the estimated datasets are considered the mean direction estimation error is around 4° in the long-crested case and 8° in the short-crested case (no wave filtering, $\hat{\Psi} > 2$).

4.2.1. *Wave filtering cases and trust measure*

In Tables 4 and 5, the cells are colored with pink when the trust measure $\hat{\Psi}$ is negative, which corresponds to the case when wave filtering is most likely occurring. In these cases, the direction estimate $\hat{\beta}$ is not satisfactory. S175 has the largest influence of wave filtering with a direction estimation error of 37° in the long-crested case and 41° in the short-crested case. The significant wave height estimate $\hat{H}_s$ oscillates significantly, and is under-estimated by almost 25%. The energy-averaged wave direction estimation procedure from the minimization of variance across the $\bar{H}_s$ columns, is a weakness of the method when wave filtering occurs. The trust measure $\hat{\Psi}$ captures the effect of wave filtering nicely in all simulation scenarios presented. This is highly useful when using the sea state estimates online in autonomous control systems. Looking at the bar charts (Figs. 5 and 6) the trend for the trust measure is for the mean value to steadily increase for higher incident wave periods, and that the smallest vessel has the highest trust value. Note that even though the trust measure is normalized with the main ship parameters, this does not necessarily mean that the trust can be compared directly between ships. The trust measure identifies when wave filtering conditions occur $\hat{\Psi} < 0$ and are likely to occur $\hat{\Psi} \in [0, 2]$. A trust measure above these values; say $\hat{\Psi} = 5$ or $\hat{\Psi} = 15$ tells us that there is little or no of wave filtering on the results. On the other hand, $\hat{\Psi} = 15$ does not automatically mean higher quality sea state estimate than when $\hat{\Psi} = 5$. When there is no wave filtering, other factors like the short-crestedness of the sea state and stationarity of the respose is important as well.

Fig. 7 shows time domain estimation results for S175 in $T_p = 8$ s in a long-crested sea state (s=50). The red lines are the incident wave parameters, the blue lines are the estimates from ten realizations, and the dashed black lines show the mean $\hat{H}_s$ and, $\hat{T}_p$ for these scenarios. It is evident that there is a lot of wave filtering happening, especially for head/following sea conditions. The estimates are improved for beam sea, which is because the projected length relative to the incident waves is smaller, i.e., the vessel is more sensitive to beam sea waves. One downside to the trust measure, in its formulation, is the fact that it is not sensitive to the relative wave direction.

If one had a reliable source of the relative wave direction, one could keep using the projected length W in the trust measure. Then one would include the heading sensitivity in the trust measure; i.e., that for beam sea the ship estimates could be perfectly adequate, whereas in head/following sea they would be degraded because of wave filtering.

Table 4
Estimation results for long-crested sea (s = 50). Mean and standard deviation calculated based on time series 2000–20000 s, including transients during heading changes. $\hat{\Psi}$ is the trust measure, with pink background when $\hat{\Psi} < 0$ (wave filtering occurs) yellow background when $\hat{\Psi} \in [0, 2]$ (chance of wave filtering) and green when $\hat{\Psi} > 2$ (little/ no wave filtering).

RV	8	10	12	14	16	18	T_p [s]
mean $\hat{H}_s$ [m]	4.1109	4.1056	4.0771	3.9228	3.9151	4.0023	
std. $\hat{H}_s$ [m]	0.3660	0.3651	0.4494	0.3454	0.4222	0.4123	
mean $\hat{T}_p$ [s]	7.9483	9.9196	11.8833	13.9453	15.7767	17.8741	
std. $\hat{T}_p$ [s]	0.4801	0.5385	0.6535	0.4840	0.7616	0.5201	
mean $\lvert\beta - \hat{\beta}\rvert$ [deg]	9.2721	12.544	15.088	15.791	16.294	19.522	
std. $\lvert\beta - \hat{\beta}\rvert$ [deg]	2.5102	2.5056	1.8785	1.6954	2.3565	2.4659	
mean $\hat{\Psi}$ [-]	2.4672	4.3620	6.6688	9.5284	12.495	16.288	
std. $\hat{\Psi}$ [-]	0.3929	0.5777	0.8444	0.7225	1.3235	0.9939	
PSV	8	10	12	14	16	18	T_p [s]
mean $\hat{H}_s$ [m]	4.1205	4.0341	3.9984	4.1111	4.0318	4.1463	
std. $\hat{H}_s$ [m]	0.3575	0.3688	0.4105	0.3494	0.4413	0.5014	
mean $\hat{T}_p$ [s]	7.8792	9.9735	12.130	13.926	15.882	17.826	
std. $\hat{T}_p$ [s]	0.5374	0.4884	0.6456	0.6671	0.9909	0.6994	
mean $\lvert\beta - \hat{\beta}\rvert$ [deg]	11.725	8.5237	9.7479	12.350	12.654	13.211	
std. $\lvert\beta - \hat{\beta}\rvert$ [deg]	9.1433	1.7810	2.7653	1.8979	1.4146	2.000	
mean $\hat{\Psi}$ [-]	0.7476	1.6761	2.9282	4.1719	5.7358	7.4299	
std. $\hat{\Psi}$ [-]	0.1808	0.2446	0.3981	0.4907	0.8335	0.6651	
S175	8	10	12	14	16	18	T_p [s]
mean $\hat{H}_s$ [m]	3.1115	3.6715	4.0733	3.9852	4.0438	4.0546	
std. $\hat{H}_s$ [m]	0.7675	0.5329	0.4248	0.4316	0.4209	0.4386	
mean $\hat{T}_p$ [s]	7.6693	9.2168	11.315	13.618	15.671	17.821	
std. $\hat{T}_p$ [s]	0.4286	0.8529	1.0329	1.1118	1.0972	0.6304	
mean $\lvert\beta - \hat{\beta}\rvert$ [deg]	37.969	23.937	17.685	22.067	15.365	16.185	
std. $\lvert\beta - \hat{\beta}\rvert$ [deg]	16.053	10.873	9.9297	9.5625	9.9090	10.873	
mean $\hat{\Psi}$ [-]	-0.4262	0.0134	0.3335	0.7840	1.275	1.8650	
std. $\hat{\Psi}$ [-]	0.0496	0.1330	0.1575	0.2057	0.2656	0.1972	

Table 5
Estimation results for short-crested sea (s=2). Mean and standard deviation calculated based on timeseries 2000–20000 s. $\hat{\Psi}$ is the trust measure, with pink background when $\hat{\Psi} < 0$ (wave filtering occurs) yellow background when $\hat{\Psi} \in [0, 2]$ (chance of wave filtering) and green when $\hat{\Psi} > 2$ (little/no wave filtering).

RV	8	10	12	14	16	18	T_p [s]
mean $\hat{H}_s$ [m]	4.1310	4.0118	3.9849	3.9432	3.9627	4.0140	
std. $\hat{H}_s$ [m]	0.3300	0.3876	0.3851	0.4094	0.4705	0.4999	
mean $\hat{T}_p$ [s]	7.8404	10.002	11.832	13.893	15.786	17.684	
std. $\hat{T}_p$ [s]	0.4634	0.5941	0.7041	0.6924	0.7584	0.8809	
mean $\lvert\beta - \hat{\beta}\rvert$ [deg]	21.201	16.590	16.781	16.490	18.890	21.134	
std. $\lvert\beta - \hat{\beta}\rvert$ [deg]	13.240	8.9609	4.8406	4.6712	4.7926	4.6478	
mean $\hat{\Psi}$ [-]	2.3813	4.4558	6.6061	9.4809	12.521	15.955	
std. $\hat{\Psi}$ [-]	0.3410	0.6136	0.8934	1.0260	1.3333	1.6460	
PSV	8	10	12	14	16	18	T_p [s]
mean $\hat{H}_s$ [m]	4.7455	4.3442	4.1308	4.0597	4.0575	4.0559	
std. $\hat{H}_s$ [m]	0.4608	0.4419	0.3825	0.3883	0.4219	0.4944	
mean $\hat{T}_p$ [s]	7.6749	9.9237	11.860	13.933	15.853	17.804	
std. $\hat{T}_p$ [s]	0.7085	0.6661	0.6502	0.6340	0.8354	0.8247	
mean $\lvert\beta - \hat{\beta}\rvert$ [deg]	20.808	15.783	22.047	17.950	15.187	17.086	
std. $\lvert\beta - \hat{\beta}\rvert$ [deg]	12.478	11.760	13.447	11.9247	5.868	4.999	
mean $\hat{\Psi}$ [-]	0.7389	1.6882	2.7602	4.1536	5.6703	7.4111	
std. $\hat{\Psi}$ [-]	0.1667	0.2777	0.4001	0.4645	0.7120	0.7403	
S175	8	10	12	14	16	18	T_p [s]
mean $\hat{H}_s$ [m]	3.0936	3.9447	4.6881	4.6404	4.2806	3.9917	
std. $\hat{H}_s$ [m]	0.6960	0.6336	0.7239	0.5063	0.5215	0.4863	
mean $\hat{T}_p$ [s]	7.5198	8.9095	10.892	13.138	15.467	17.881	
std. $\hat{T}_p$ [s]	0.4788	0.8627	1.1940	1.5423	1.2952	0.8325	
mean $\lvert\beta - \hat{\beta}\rvert$ [deg]	41.522	30.646	24.910	22.582	19.659	20.051	
std. $\lvert\beta - \hat{\beta}\rvert$ [deg]	11.583	12.862	14.572	15.536	14.586	15.267	
mean $\hat{\Psi}$ [-]	-0.4288	-0.0525	0.3203	0.7654	1.2588	1.8937	
std. $\hat{\Psi}$ [-]	0.0522	0.1139	0.1618	0.1679	0.2152	0.2458	

Taking S175 in a sea state with $T_p = 8$ s as an example, the trust measure for beam sea, using B in stead of L, is $\hat{\Psi} = \left(\frac{\lambda - B}{L}\right) = 0.425$ whereas the trust measure in head sea $\hat{\Psi} = \left(\frac{\lambda - L}{L}\right) = -0.429$. $\hat{\Psi} = 0.425$ still indicates that there is some wave filtering occurring, however to a smaller extent than in head sea conditions.

When the trust measure is close to zero, there is a chance of wave filtering occurring, since there are many wave components that have period above $\hat{T}_p$. In the tables with statistics (Tables 4 and 5), this is indicated by coloring the cells yellow when $\hat{\Psi} \in [0, 2]$. In these cases, the direction estimation error is increased to the range 15–17° in the long-crested case and 20–22° in the short-crested case. The impact of the wave filtering is not evident in the significant wave height estimates before $\hat{\Psi} < 0.5$. The standard deviation of the estimated wave parameters are small for the case of no wave filtering, and is

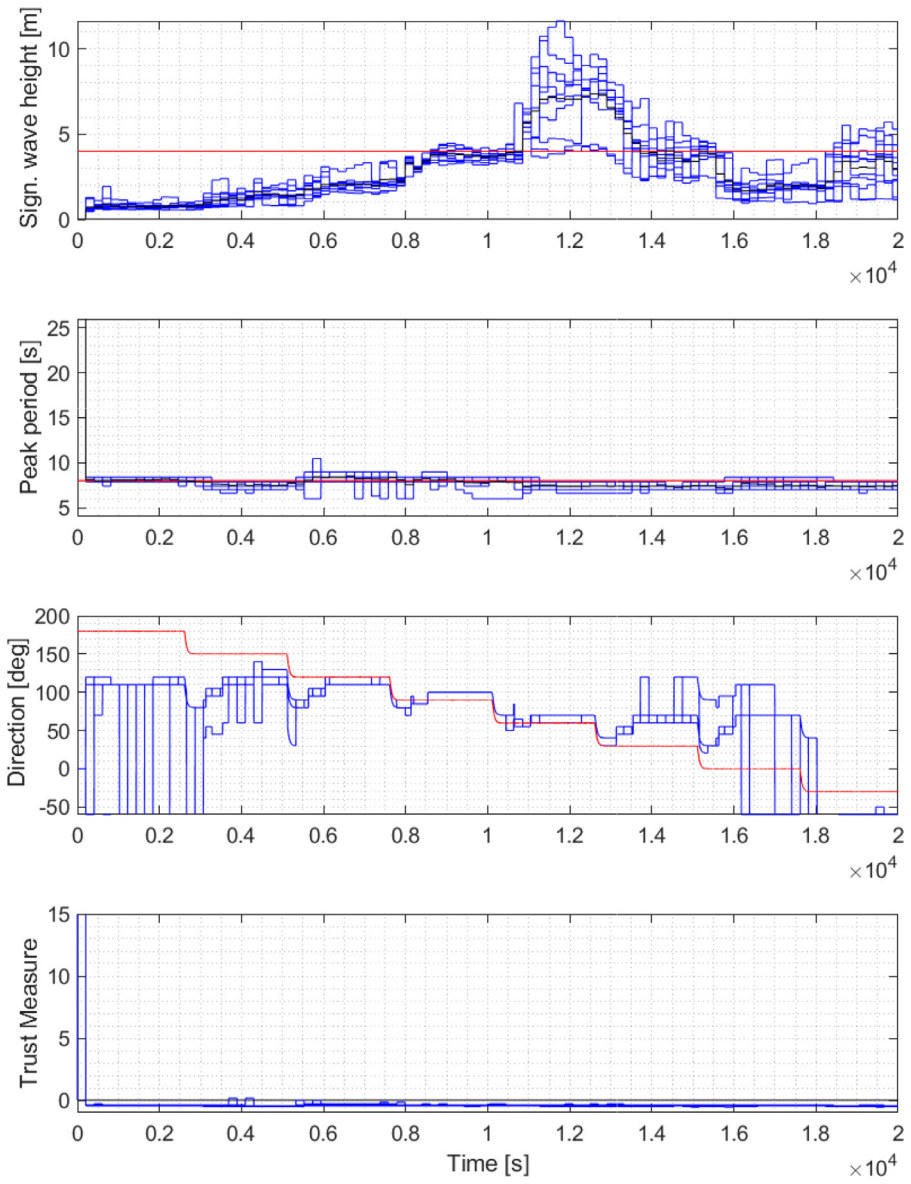

Fig. 7. Sea state estimation results for 10 realizations, S175 $T_p = 8$ s, spread $s = 50$, long-crested sea. High influence of wave filtering. The red lines are the incident wave parameters, the blue lines are the estimates from ten realizations, and the dashed black lines show the mean $\hat{H}_s$ and, $\hat{T}_p$ for these scenarios. (For interpretation of the references to color in this figure legend, the reader is referred to the web version of this article.)

larger when wave filtering occurs, see Fig. 5 for a bar chart. This is not surprising, as in the case of wave filtering, the incident wave elevation time series (calculated based on the randomized direction, frequency and phase) has a significant effect on how the vessel responds. For instance, a wave train followed by some time with calm sea will make the sea state estimates vary more, than if the ship response was sensitive to most of the incident wave components.

4.2.2. Directional spread of incident waves

Previously the algorithm has been tested in completely long-crested sea (no directional spread), and on a limited full scale dataset with small directional spread. A realistic sea state will have some directional spread, so therefore two different spreads were tested in these simulations. Apart from the cases with wave filtering, the estimated relative wave direction is consistent at around 13° off the true direction for the long-crested scenario. The estimation error for the short-crested case is larger at around 16° (where there is no wave filtering $\hat{\Psi} > 2$.

The estimated wave direction is degraded when the sea state is short-crested, however, the directional spread of the incident waves had surprisingly little to say in the simulated scenarios. Perhaps there were too few randomized wave elevations to draw a definite conclusion on the influence of directional spread. There was some more difficulty in determining $\hat{\beta}$ for S175 with the $T_p = 8$ s in short-crested sea. However, for this case the estimated relative wave direction was never estimated reliably, due to significant wave filtering. However, it is emphasized that this formulation of the algorithm will not give an estimate of directional spread. If this is of importance for the application, the simplified approach is formulated for short-crested sea in Nielsen et al. (2018) or a more comprehensive sea state estimation model should be used, for instance the Bayesian approach described in Nielsen (2008).

The reason for this large degradation of the direction estimates comes from the energy-averaged methodology. It is thought that if the direction estimate was assisted by multiple distributed sensors, the direction estimate resolution may be improved significantly without increasing the computational burden noticeably. By using this type of approach it is also thought that the direction estimate would be more robust for wave filtering cases. A distributed sensing strategy requires

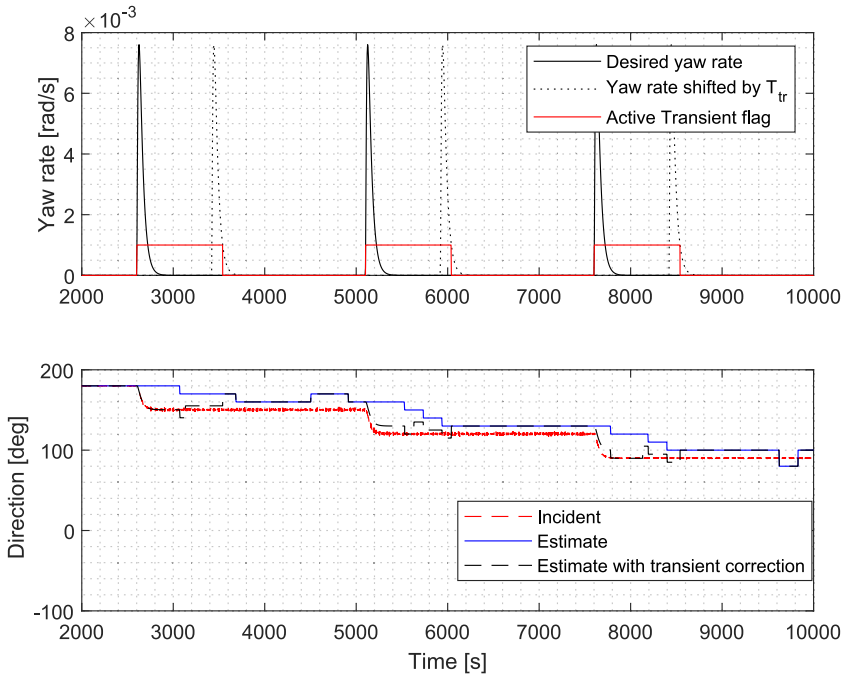

Fig. 8. Illustration of the relative wave direction correction during transients due to heading changes (Case: PSV, $T_p = 10$ s, short-crested sea, spread $s = 2$).

a minimum of three non-colinear sensors in order to have observability (Dirdal et al., 2022). It is noteworthy that sensor alignment is very important for the estimation results.

4.2.3. Transients due to heading changes

On a whole, the transients due to heading changes in this simulation study did not affect the certainty of the H_s and T_p estimates noticeably. The reason being that $\hat{H}_s$ and $\hat{T}_p$ originate from the heave response, and the heave response is less sensitive to relative wave direction than roll and pitch. The direction estimate $\hat{\beta}$ lagged by the same time as the window used for FFT, stepping down towards the new β. The lag was effectively corrected for by using the heading measurements of the vessel when a heading change was commanded, and for T_{tr} seconds afterwards, see Eq. (22). The transient correction of the relative wave direction estimate is illustrated in Fig. 8. The desired yaw rate, the desired yaw rate shifted forward by T_{tr} seconds, and the transient flag are plotted in the upper plot. In the lower plot, the true incident relative wave direction, the estimated relative wave direction, and the estimated relative wave direction with correction during transients is shown.

It must be emphasized that the sea state estimation algorithm requires that the time series are stationary for the most part. A period in steady state followed by a relatively fast change in heading, and resuming steady state for a longer period in time is acceptable. A series of heading changes without sufficient steady state response in between will quickly deteriorate the results. Recall, that it takes T_{tr} seconds, here 820 s (13 min), before a transient is completely eliminated from the response spectral calculations. Continuing on this thought, a downside to this heading-correction strategy, is that in the case where the heading estimate is wrong at the time a new heading change is commanded, then the estimate will be kept wrong for a significant amount of time.

4.2.4. Influence of wave elevation randomness

It was noticed in the study (Brodtkorb et al., 2018b) that the significant wave height was over-estimated quite significantly for the entire time series. The stochastic wave realization and energy in the wave system is believed to have a role in this. From the present study, it is found that the variation of the (stochastic) wave realization was the single most important parameter influencing the shorter-term wave elevation and vessel response, and hence the sea state estimates. This is also a finding supported in Nielsen et al. (2022). When using a large time window with many samples ($N_{FFT} \to \infty$), the surface elevation will statistically be given by the input sea state parameters (H_s, T_p, direction and spread). However, when using smaller number of samples, e.g., $N_{FFT} = 4096$, then the wave elevation is not (necessarily) described well by the statistical parameters. In these simulations, the random seed for the wave elevation time series had more to say than the violation of stationary conditions, and the directional spread of the waves.

4.3. Benchmarking study

As already indicated, several methods have been developed for sea state estimation, considering the ship as a sailing wave buoy. In terms of the produced output, the most complete estimate is given by the directional wave spectrum. It is important to note, however, that solving for the directional wave spectrum leads to a more demanding mathematical problem since it requires consideration of all frequency-directional spectral densities, in contrast to Eq. (1) which is a function of only frequency. This means that the number of unknowns, as a rule of thumb, at least doubles when applying, e.g. the Bayesian (non-parametric) method described in Nielsen (2008). In addition to this, regularization ("smoothing constraints") must be introduced, resulting in a mathematical problem which in turn must be solved in a multiple iterative manner that completes by minimization of an objective criterion (Akaike, 1980). Suffice it to say that, while the Bayesian method is recognized for yielding good wave spectrum estimates, it is also a method with a relatively high algorithmic complexity necessitating a large number of computational operations. To this end, the Bayesian method probably yields the most elaborate estimate available, when applying and analyzing the wave buoy analogy, but the method is associated with a large computational burden that may be beyond the requirements of an online control system used for DP operations, not to mention that its output, i.e. the directional wave spectrum, is far more detailed than what is required for, e.g., tuning gains of a DP control system. Nevertheless, in the following, the output of the proposed algorithm is assessed by benchmarking against the best possible estimate, as obtained from the Bayesian method.

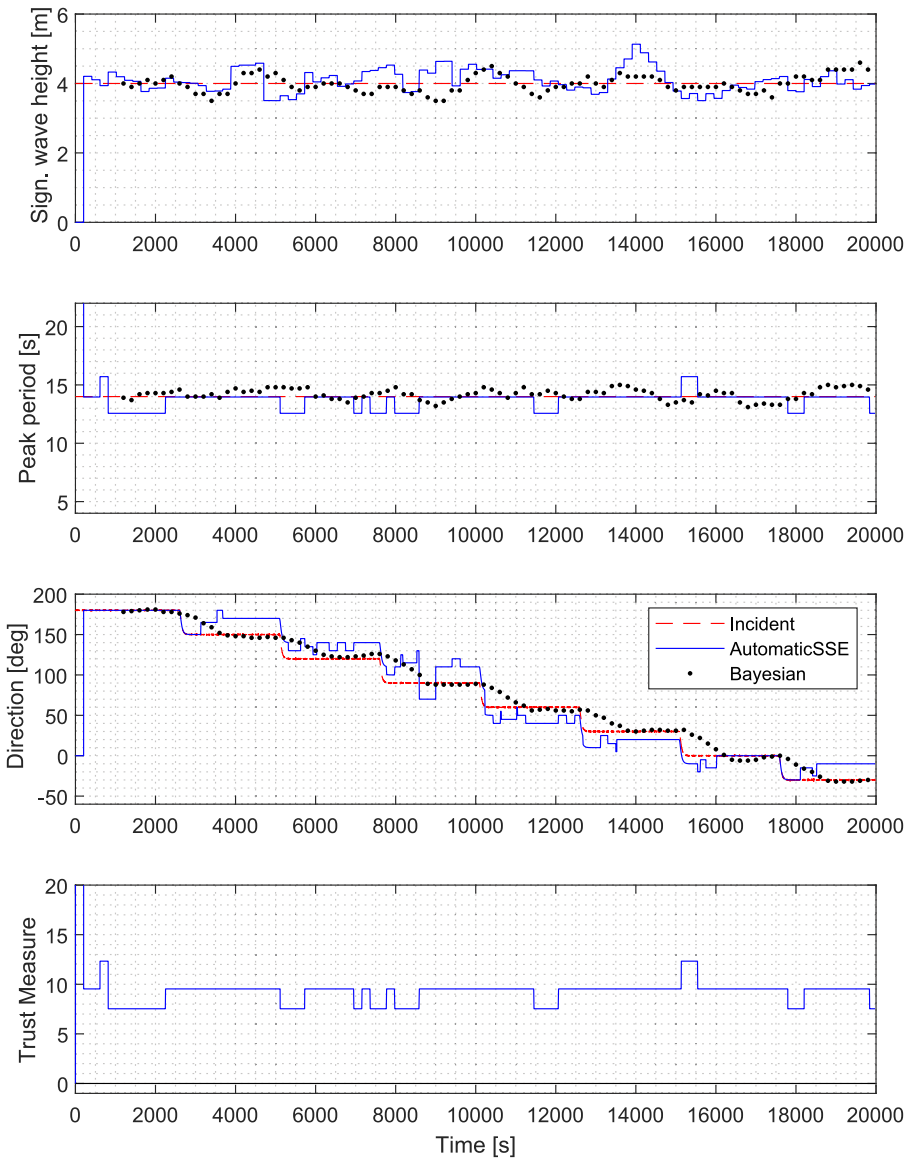

Fig. 9. Benchmarking study results for RV, Spread = 2, Tp = 14 s. Red dashed line are incident parameters, the blue line is the method proposed in this paper, and the black dots is the Bayesian approach. (For interpretation of the references to color in this figure legend, the reader is referred to the web version of this article.)

Figs. 9–11 show the estimates from the automatic wave estimation algorithm (blue) and the Bayesian approach (black dots) plotted against time. In this case, the waves are short-crested, with a directional spread of 2, and the influence of wave filtering is minimal. In general the wave parameters are estimated with similar uncertainties for the two procedures, which is encouraging. It is no surprise that the Bayesian approach has more precise estimates that vary less with time. This is due to the fact that the Bayesian approach solves the more complex problem of frequency-directional spectral densities, and in addition includes smoothing on the produced 2D wave spectra. Above all, the noteworthy point is that the simplified algorithm proposed in this paper follows the trends in the wave parameters well. The direction estimation is generally a bit worse for the simplified algorithm. This has to do with the energy-comparison procedure for identifying the direction, not to mention that the algorithm is limited to estimating directions with a discretization of 10°. Notice that the Bayesian approach can estimate all directions.

The largest differences between the results occur when there is significant wave filtering, see Fig. 12. The Bayesian approach is also affected negatively by wave filtering, but has considerably better estimates of the energy in the wave system and wave direction. The main problem with wave filtering is the removal of information about the waves from the vessel response measurements. The only way to truly improve the estimation results during wave filtering, is to add a second sensor, e.g. wave probes (Souza, 2019), in order to improve the observability for smaller waves relative to the vessel size.

In an autonomous ship control system, both the automatic sea state estimation algorithm and the Bayesian approach can be used simultaneously to improve the situational awareness of the control system, as well as supervising operators. The simplified approach can provide wave parameter estimates to be used directly in online control functionality, while supervised by the Bayesian approach, which gives more accurate and elaborate estimates of the 2D wave spectra and associated wave parameters periodically, e.g., every half hour. In the case where the two estimation methods produce conflicting results, the operator may be informed, and may be prompted to intervene in the operation.

5. Conclusion

A computationally efficient sea state estimation algorithm was presented; providing precise and consistent estimates of the onsite 1D wave

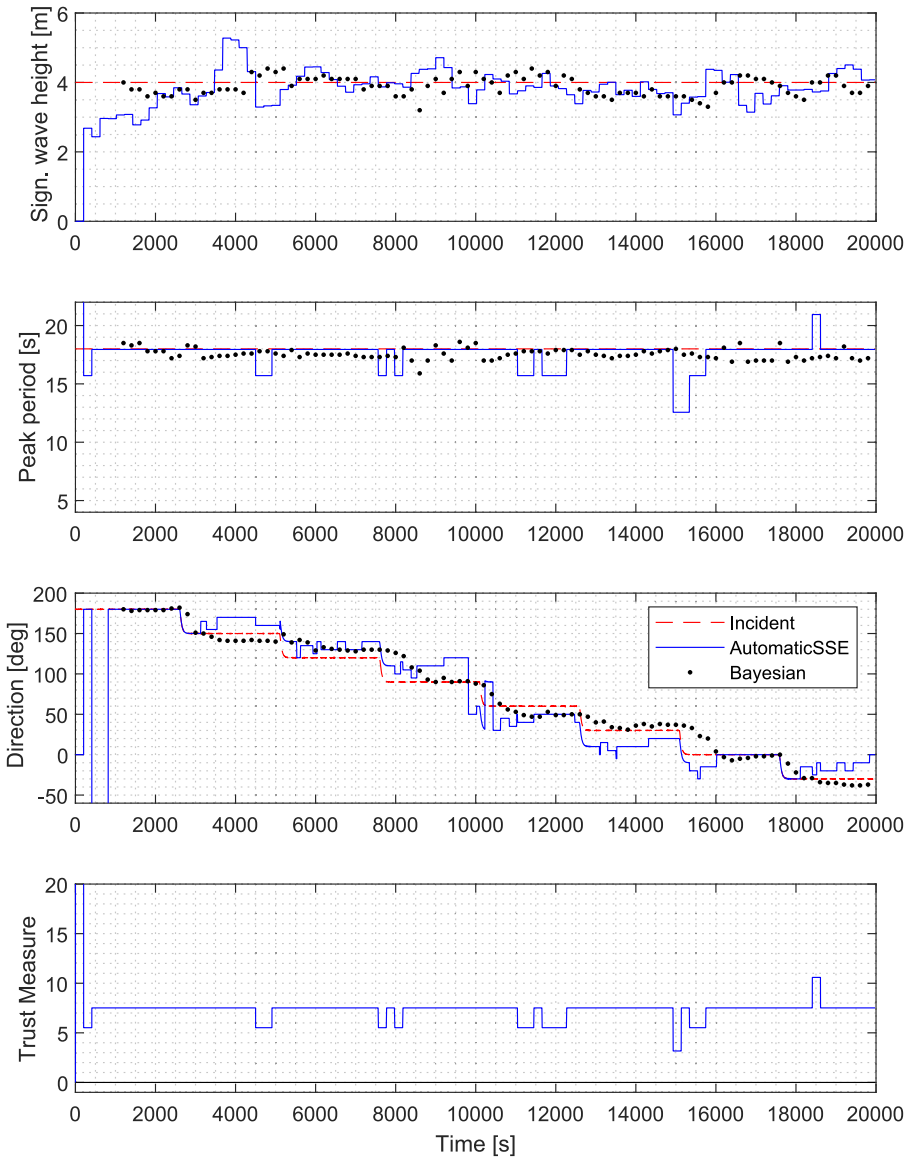

Fig. 10. Benchmarking study results for PSV, Spread = 2, Tp = 18 s. Red dashed line are incident parameters, the blue line is the method proposed in this paper, and the black dots is the Bayesian approach. (For interpretation of the references to color in this figure legend, the reader is referred to the web version of this article.)

spectrum and associated wave parameters ($\hat{S}; \hat{H}_s, \hat{T}_p, \hat{\beta}$). Automatic gain and tolerance calculations worked as anticipated, making the procedure low-effort for implementing on different vessels, and there was no tuning required for different wave conditions. The trust measure $\hat{\Psi}$ captures the effect of wave filtering nicely in all simulation scenarios presented, indicating when the estimates are to be trusted and not. In the current state is it not sensitive to the relative wave direction, which is something that could be done in the case where a redundant and reliable wave direction estimate/measurement exists. The sea state estimates corresponded well with state-of-the-art Bayesian estimation approach. This indicates that the simplifications made in order to enhance the computational speed, has not affected the quality of the estimates noteworthy.

Directions for further work include improving the energy-averaged direction estimate, especially for cases when wave filtering occurs, as well as extending the algorithm to the case with non-zero forward speed.

Declaration of competing interest

The authors declare that they have no known competing financial interests or personal relationships that could have appeared to influence the work reported in this paper.

Acknowledgments

This work was supported by the Research Council of Norway through the Centres of Excellence funding scheme, grant number 223254 - NTNU AMOS.

Appendix. Stability analysis

The following section is taken from Brodtkorb et al. (2018b). In order to find suitable values for the gains h_{ij}, the sea state estimation error dynamics are analyzed using discrete Lyapunov analysis.

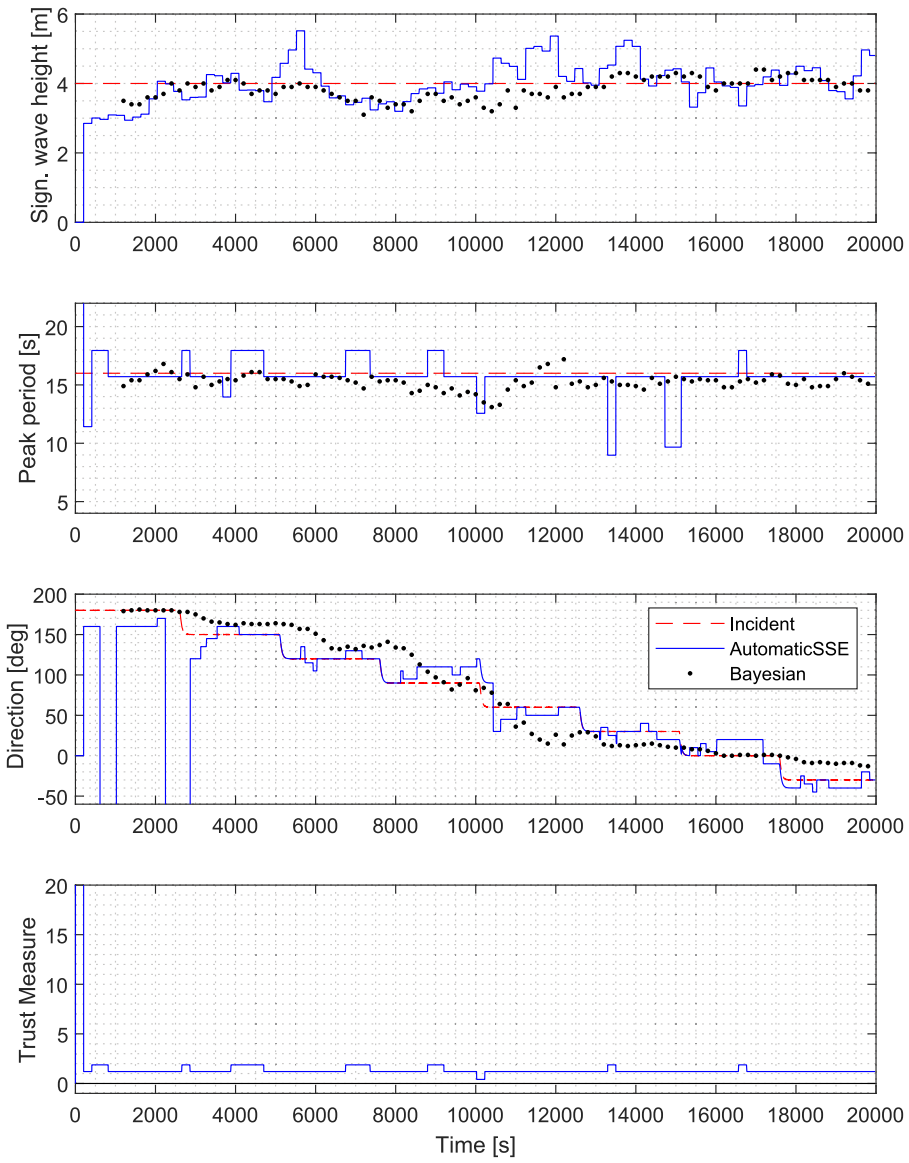

Fig. 11. Benchmarking study results for S175, Spread = 2, Tp = 16 s. Red dashed line are incident parameters, the blue line is the method proposed in this paper, and the black dots is the Bayesian approach. (For interpretation of the references to color in this figure legend, the reader is referred to the web version of this article.)

Error dynamics

The wave spectrum estimation error is

$$\tilde{S}_{ij}(\omega,k) := S(\omega) - \hat{S}_{ij}(\omega,k) \tag{A.1}$$

The estimation error dynamics are derived in the following:

$$\tilde{S}^{+}_{ij}(\omega,k) = S^{+}(\omega) - \hat{S}^{+}_{ij}(\omega,k) \tag{A.2a}$$

$$= S(\omega) - \hat{S}_{ij}(\omega,k) - h_{ij}\tilde{R}_{ij}(\omega,k) \tag{A.2b}$$

It has been inserted that the wave spectrum does not change over time, so that $S^{+}(\omega) = S(\omega)$, see Eq. (4). By using (5)b inserted into (5)a, $\tilde{R}_{ij}$ can be written as:

$$\tilde{R}_{ij}(\omega,k) = \left|X_i(\omega,k)\overline{X_j(\omega,k)}\right|\left(S(\omega) - \hat{S}_{ij}(\omega,k)\right) \tag{A.3}$$

$$= \left|X_i(\omega,k)\overline{X_j(\omega,k)}\right|\tilde{S}_{ij}(\omega,k) \tag{A.4}$$

The error dynamics are

$$\tilde{S}^{+}_{ij}(\omega,k) = \left(1 - h_{ij}\left|X_i(\omega,k)\overline{X_j(\omega,k)}\right|\right)\tilde{S}_{ij}(\omega,k). \tag{A.5}$$

This is a linear, unforced, system where the system matrix $\left(1 - h_{ij}\left|X_i(\omega,k)\overline{X_j(\omega,k)}\right|\right)$ is independent of time.

Lyapunov analysis

Proposition 1. *Given that the iteration gain h_{ij} is chosen as*

$$h_{ij} < \frac{2}{\left|X_i(\omega,k)\overline{X_j(\omega,k)}\right|}, \quad ij = \{zz, \phi\phi, \theta\theta, z\phi, z\theta, \phi\theta\},$$

and assumptions (A1)–(A3) hold (see Section 2), the origin of the wave spectrum estimation error dynamics Eq. (A.5) is discrete-time uniformly asymptotically stable in the large. □

In order to simplify the notation of the proof, the arguments (ω,k) are left out from the equations.

Proof. Using results for discrete-time systems from Kalman and Bertram (1960), Theorem 1*. The following Lyapunov function candidate is proposed:

$$V(\tilde{S}_{ij}) := \frac{1}{2}\tilde{S}^{2}_{ij}. \tag{A.6}$$

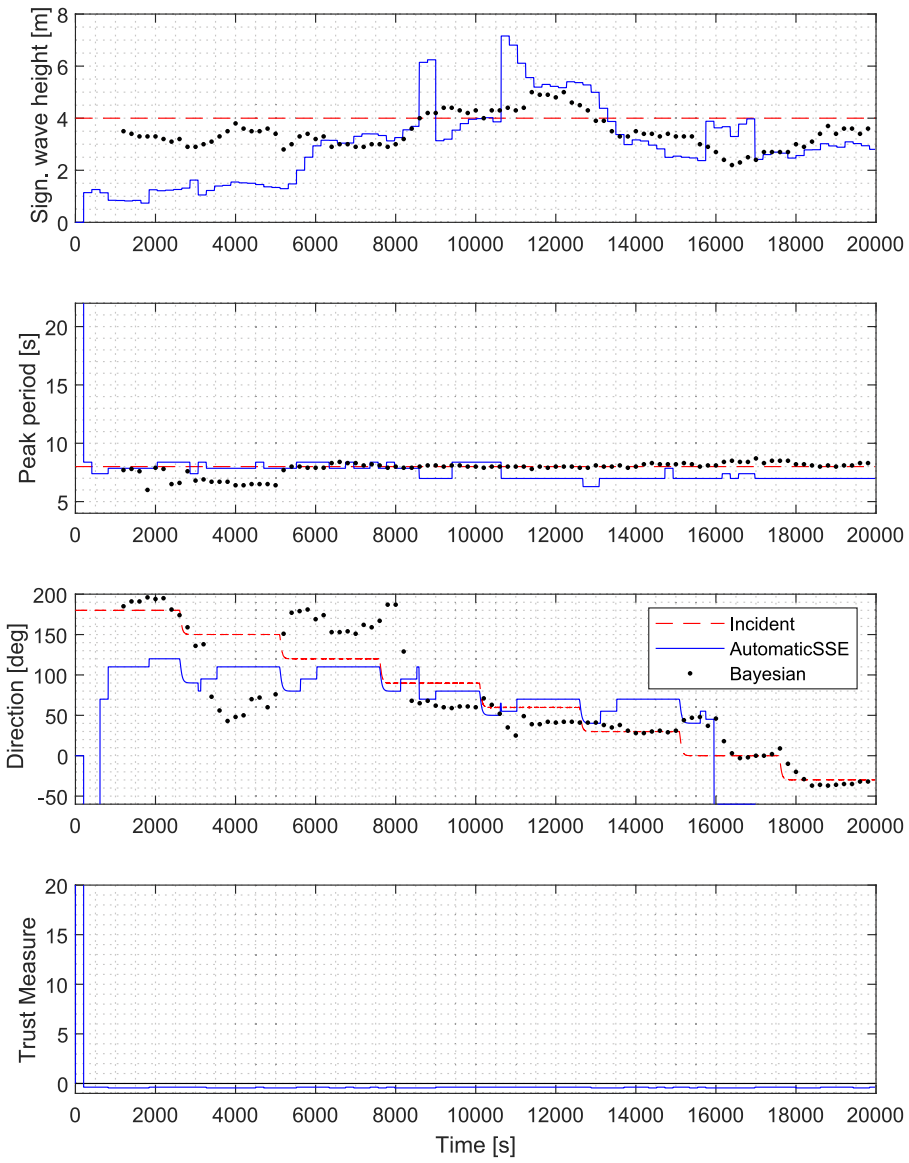

Fig. 12. Benchmarking study results for S175, Spread = 2, Tp = 8 s. Red dashed line are incident parameters, the blue line is the method proposed in this paper, and the black dots is the Bayesian approach. Significant wave filtering. (For interpretation of the references to color in this figure legend, the reader is referred to the web version of this article.)

$V(\tilde{S}_{ij})$ is a continuous function of $\tilde{S}_{ij}$, with $V(0) = 0$.

(i) $0 < \alpha(\|\tilde{S}_{ij}\|) \leq V(\tilde{S}_{ij})$, with $\alpha(\|\tilde{S}_{ij}\|) := \frac{1}{4}\|\tilde{S}_{ij}\|^2$.

(ii) Need to show that the Lyapunov function is decreasing with discrete time:

$$V(\phi(\tilde{S}_{ij})) - V(\tilde{S}_{ij}) \leq -\gamma(\|\tilde{S}_{ij}\|), \tag{A.7}$$

with $\phi(\tilde{S}_{ij})$ denoting the jump map (next value) of $\tilde{S}_{ij}$ Eq. (A.5), and $\gamma(\cdot)$ being a positive definite function (non-decreasing) with $\gamma(0) = 0$. Inserting the system error dynamics gives:

$$V(\phi(\tilde{S}_{ij})) - V(\tilde{S}_{ij}) = \frac{1}{2}(\tilde{S}_{ij}^{+})^2 - \frac{1}{2}\tilde{S}_{ij}^2 \tag{A.8a}$$

$$= \frac{1}{2}\left(1 - h_{ij}\left|X_i\overline{X}_j\right|\right)^2 \tilde{S}_{ij}^2 - \frac{1}{2}\tilde{S}_{ij}^2 \tag{A.8b}$$

$$= h_{ij}\left|X_i\overline{X}_j\right|\left(\frac{1}{2}h_{ij}\left|X_i\overline{X}_j\right| - 1\right)\tilde{S}_{ij}^2 \tag{A.8c}$$

$$\leq h_{ij}\left|X_i\overline{X}_j\right|\left(\frac{1}{2}h_{ij}\left|X_i\overline{X}_j\right| - 1\right)\|\tilde{S}_{ij}\|^2 \tag{A.8d}$$

$$= -\gamma(\|\tilde{S}_{ij}\|) \tag{A.8e}$$

(iii) $V(\tilde{S}_{ij}) \leq \beta(\|\tilde{S}_{ij}\|)$, $\beta(\tilde{S}_{ij}) = \|\tilde{S}_{ij}\|^2$.

(iv) $\alpha(\|\tilde{S}_{ij}\|) \to \infty$ when $\|\tilde{S}_{ij}\| \to \infty$. □

References

Akaike, H. (1980). Likelihood and Bayes procedure. In J. Bernado, M. De Groot, D. Lindley, & A. Smith (Eds.), *Bayesian statistics* (pp. 143–166). Valencia: University Press.

Belleter, D. J. W., Galeazzi, R., & Fossen, T. I. (2015). Experimental verification of a global exponential stable nonlinear wave encounter frequency estimator. *Ocean Engineering, 97*, 48–56.

Billings, G., Walter, M., Pizarro, O., Johnson-Roberson, M., & Camilli, R. (2021). Towards automated sample collection and return in extreme underwater environments. ArXiv:2112.15127.

Brodtkorb, A. H., Nielsen, U. D., & Sørensen, A. J. (2018a). -Sea state estimation using vessel response in dynamic positioning. *Applied Ocean Research, 70*, 76–86.

Brodtkorb, A. H., Nielsen, U. D., & Sørensen, A. J. (2018b). Online wave estimation using vessel motion measurements, project number 223254 - NTNU amos. *IFAC-PapersOnLine, 51*(29), 244–249, 11th IFAC Conference on Control Applications in Marine Systems, Robotics, and Vehicles CAMS 2018.

Chen, J., Pillai, A. C., Johanning, L., & Ashton, I. (2021). Using machine learning to derive spatial wave data: A case study for a marine energy site. *Environmental Modelling and Software, 142*, Article 105066.

Cheng, X., Li, G., Skulstad, R., Chen, S., Hildre, H. P., & Zhang, H. (2019). Modeling and analysis of motion data from dynamically positioned vessels for sea state estimation. In *2019 international conference on robotics and automation* (pp. 6644–6650).

Dah-Jing Jwo, I.-H. W. (2021). Windowing techniques, the welch method for improvement of power spectrum estimation. *Computers, Materials & Continua*, *67*(3), 3983–4003.

Dallolio, A., Alfredsen, J. A., Fossen, T. I., & Johansen, T. A. (2021). Experimental validation of a nonlinear wave encounter frequency estimator onboard a wave-propelled USV. In *13th IFAC conference on control applications in marine systems, robotics, and vehicles*.

Dallolio, A., Quintana-Diaz, G., Honoré-Livermore, E., Garrett, J. L., Birkeland, R., & Johansen, T. A. (2021). A satellite-USV system for persistent observation of mesoscale oceanographic phenomena. *Remote Sensing*, *13*(16).

Dirdal, J. A., Skjetne, R., Roháč, J., & Fossen, T. I. (2022). Online wave direction and wave number estimation from surface vessel motions using distributed inertial measurement arrays and phase-time-path-differences. *Ocean Engineering*, *249*, Article 110760.

Duz, B., Mak, B., Hageman, R., & Grasso, N. (2021). Real time estimation of local wave characteristics from ship motions using artificial neural networks. *Lecture Notes in Civil Engineering*, *65*, 657–678.

Fossen, T. I. (2011). *Handbook of marine craft hydrodyamics and motion control*. Wiley.

Han, X., Leira, B. J., & Sævik, S. (2021). Vessel hydrodynamic model tuning by discrete Bayesian updating using simulated onboard sensor data. *Ocean Engineering*, *220*, Article 108407.

Iseki, T. (2010). Real-time analysis of higher order ship motion spectrum. In *ASME. 29th international conference on ocean, offshore and arctic engineering, Vol. 2* (pp. 399–405).

Iseki, T., & Ohtsu, K. (2000). Bayesian estimation of directional wave spectra based on ship motions. *Control Engineering Practice*, *8*(2), 215–219.

Jensen, J. J. (2001). Load and global response of ships. *Elsevier Science*, *4*, 151–152.

Kalman, R. E., & Bertram, J. E. (1960). Control system analysis and design via the second method of Lyapunov: II— discrete-time systems. *ASME. Journal of Basic Engineering*, *82*, 394–400.

Montazeri, N., Nielsen, U. D., & Jensen, J. J. (2016). Estimation of wind sea and swell using shipboard measurements – a refined parametric modelling approach. *Applied Ocean Research*, *54*, 73–86.

Mounet, R. E., Nielsen, U. D., Brodtkorb, A. H., Tannuri, E. A., & de Mello, P. C. (2022). Simultaneous sea state estimation and transfer function tuning using a network of dynamically positioned ships. *Applied Ocean Research*, *129*, Article 103367.

Nielsen, U. D. (2005). *Estimation of directional wave spectra from measured ship responses*. (Ph.D. thesis), May: Section of Coastal, Maritime and Structural Engineering, Department of Mechanical Engineering, Technical University of Denmark.

Nielsen, U. D. (2007). Response-based estimation of sea state parameters - influence of filtering. *Ocean Engineering*, *34*(13), 1797–1810.

Nielsen, U. D. (2008). Introducing two hyperparameters in Bayesian estimation of wave spectra. *Probabilistic Engineering Mechanics*, *23*(1), 84–94.

Nielsen, U. D. (2017). A concise account of techniques available for shipboard sea state estimation. *Ocean Engineering*, *129*, 352–362.

Nielsen, U. D., Bjerregård, M., Galeazzi, R., & Fossen, T. I. (2015). New concepts for shipboard sea state estimation. In *MTS/IEEE oceans*. Washington DC.

Nielsen, U. D., Brodtkorb, A. H., & Sørensen, A. J. (2018). A brute-force spectral approach for wave estimation using measured vessel responses. *Marine Structures*.

Nielsen, U. D., Brodtkorb, A. H., & Sørensen, A. J. (2019). Sea state estimation using multiple ships simultaneously as sailing wave buoys. *Applied Ocean Research*, *83*, 65–76.

Nielsen, U. D., Mounet, R. E., & Brodtkorb, A. H. (2021). Tuning of transfer functions for analysis of wave–ship interactions. *Marine Structures*, *79*, Article 103029.

Nielsen, U. D., Mounet, R. E. G., & Brodtkorb, A. H. (2022). Parameterised transfer functions with associated confidence bands. *Applied Ocean Research*, *125*, 2022.

Pascoal, R., Guedes Soares, C., & Sørensen, A. J. (2007). Ocean wave spectral estimation using vessel wave frequency motions. *Journal of Offshore Mechanics and Arctic Engineering*, *129*(2), 90–96.

Pascoal, R., Perera, L., & Guedes Soares, C. (2017). Estimation of directional sea spectra from ship motions in sea trials. *Ocean Engineering*, *132*, 126–137.

Reddy, N. P., Zadeh, M. K., Thieme, C. A., Skjetne, R., Sørensen, A. J., Aanondsen, S. A., Breivik, M., & Eide, E. (2019). Zero-emission autonomous ferries for urban water transport: Cheaper, cleaner alternative to bridges and manned vessels. *IEEE Electrification Magazine*, *7*(4), 32–45.

Ren, Z., Han, X., Verma, A. S., Dirdal, J. A., & Skjetne, R. (2021). Sea state estimation based on vessel motion responses: Improved smoothness and robustness using Bézier surface and L1 optimization. *Marine Structures*, *76*, Article 102904, URL https://www.sciencedirect.com/science/article/pii/S0951833920301969.

Scholcz, T. P., & Mak, B. (2020). Ship as a wave buoy: Estimating full directional wave spectra from in-service ship motion measurements using deep learning. In *International conference on offshore mechanics and arctic engineering, volume 1: offshore technology*. 2020.

Simos, A. N., Sparano, J. V., Tannuri, E. A., & Matos, V. L. F. (2007). Directional wave spectrum estimation based on a vessel 1st order motions: Field results. In *Proceedings of the international offshore and polar engineering conference* (pp. 1938–1944).

Sintef Ocean (2017). Shipx. Trondheim, Norway, http://www.sintef.no/programvare/shipx/.

Souza, F. L. (2019). *Bayesian estimation of directional wave spectrum using vessel movements and wave-probes*. (Doctoral Thesis), Escola Politécnica: University of São Paulo, São Paulo.

Stredulinsky, D., & Thornhill, E. (2011). Ship motion and wave radar data fusion for shipboard wave measurement. *Journal of Ship Research*, *55*, 73–85.

Takami, T., Nielsen, U. D., Xi, C., Jensen, J. J., & Oka, M. (2022). Reconstruction of incident wave profiles based on short-time ship response measurements. *Applied Ocean Research*, *123*, Article 103183.

Tannuri, E., Sparano, J., Simos, A., & Da Cruz, J. (2003). Estimating directional wave spectrum based on stationary ship motion measurements. *Applied Ocean Research*, *25*(5), 243–261.

Thieme, C. A., Rokseth, B., & Utne, I. B. (2021). Risk-informed control systems for improved operational performance and decision-making. *Proceedings of the Institution of Mechanical Engineers, Part O: Journal of Risk and Reliability*, 1748006X211043657.

Toshiki, K., Kawamura, Y., Okada, T., Mitsuyuki, T., & Chen, X. (2021). Sea state estimation using monitoring data by convolutional neural network (CNN) (2021). *Journal of Marine Science and Technology*, *26*.

Udjus, G. (2017). *Force field identification and positioning control of an autonomous vessel using inertial measurement units*. (Master's thesis), Supervisor: Roger Skjetne: Department of Marine Technology, NTNU.

Værnø, S. A., Brodtkorb, A. H., Skjetne, R., & Calabrò, V. (2017). Time-varying model-based observer for marine surface vessels in dynamic positioning. *IEEE Access*, *5*, 14787–14796.

Welch, P. D. (1967). The use of fast Fourier transform for the estimation of power spectra: A method based on time averaging over short modified periodograms. *IEEE Transactions on Audio and Electroacoustics*, *15*, 70–73.

Wu, M., & Gao, Z. (2021). Methodology for developing a response-based correction factor (alpha-factor) for allowable sea state assessment of marine operations considering weather forecast uncertainty. *Marine Structures*, *79*, Article 103050.